

Document downloaded from:

<http://hdl.handle.net/10251/146886>

This paper must be cited as:

Martín, G.; Rovira, A.; Veciana, N.; Soy, J.; Toledo, G.; Gommers, C.; Boix, M.... (2018). Circadian waves of transcriptional repression shape PIF-regulated photoperiod-responsive growth in Arabidopsis. *Current Biology*. 28(2):311-318.
<https://doi.org/10.1016/j.cub.2017.12.021>



The final publication is available at

<https://doi.org/10.1016/j.cub.2017.12.021>

Copyright Elsevier

Additional Information

1 **Circadian waves of transcriptional repression shape PIF-regulated photoperiod-**
2 **responsive growth in Arabidopsis**

3 Guiomar Martín¹, Arnau Rovira¹, Nil Veciana¹, Judit Soy¹, Gabriela Toledo-Ortiz^{3,4},
4 Charlotte M. M. Gommers¹, Marc Boix¹, Rossana Henriques¹, Eugenio G. Minguet²,
5 David Alabadi², Karen Halliday⁴, Pablo Leivar^{1,5}, and Elena Monte^{1,6,7,*}

6 ¹Center for Research in Agricultural Genomics (CRAG), CSIC-IRTA-UAB-UB, Campus
7 UAB, Edifici CRAG, Bellaterra, 08193 Barcelona, Spain.

8 ²Instituto de Biología Molecular y Celular de Plantas (IBMCP), CSIC-UPV, Ingeniero
9 Fausto Elio s/n, 46022 Valencia, Spain

10 ³Lancaster Environment Center, Lancaster University. Lancaster, LA1 4YQ, UK.

11 ⁴The University of Edinburgh. CH Waddington Building, Max Born Crescent,
12 Edinburgh, EH9 3BF, UK.

13 ⁵Bioengineering Department, IQS School of Engineering. Via Augusta 390, 08017
14 Barcelona, Spain.

15 ⁶Consejo Superior de Investigaciones Científicas (CSIC), 08028 Barcelona, Spain.

16 ⁷Lead contact

17 *Corresponding author: elena.monte@cragenomica.es

18

19 **Summary**

20 Plants coordinate their growth and development with the environment through integration
21 of circadian clock and photosensory pathways. In *Arabidopsis thaliana*, rhythmic
22 hypocotyl elongation in short days (SD) is enhanced at dawn by the bHLH transcription
23 factors PHYTOCHROME-INTERACTING FACTORS (PIFs) directly inducing
24 expression of growth-related genes [1–6]. PIFs accumulate progressively during the night
25 and are targeted for degradation by active phytochromes in the light, when growth is
26 reduced. Although PIF proteins are also detected during the day hours [7–10], their
27 growth-promoting activity is inhibited through unknown mechanisms. Recently, the core
28 clock components and transcriptional repressors PSEUDO-RESPONSE REGULATORS
29 PRR9/7/5 [11,12], negative regulators of hypocotyl elongation [13,14], were described to
30 associate to G-boxes [15], the DNA motifs recognized by the PIFs [16,17], suggesting
31 that PRR and PIF function might converge antagonistically to regulate growth. Here we
32 report that PRR9/7/5 and PIFs physically interact and bind to the same promoter region
33 of pre-dawn-phased, growth-related genes, and we identify the transcription factor CDF5
34 [18,19] as target of this interplay. In SD, *CDF5* expression is sequentially repressed from
35 morning to dusk by PRRs and induced pre-dawn by PIFs. Consequently, *CDF5*
36 accumulates specifically at dawn, when it induces cell elongation. Our findings provide a
37 framework for recent TIMING OF CAB EXPRESSION 1 (TOC1/PRR1) data [5,20] and
38 reveal that the long described circadian morning-to-midnight waves of the PRR
39 transcriptional repressors (PRR9, PRR7, PRR5 and TOC1) [21] jointly gate PIF activity
40 to dawn to prevent overgrowth through sequential regulation of common PIF-PRR target
41 genes such as *CDF5*.

42

43 **Results and Discussion**

44 Genome-wide analysis of ChIP-sequencing (ChIP-seq) data for the PIF quartet (PIFq)
45 (PIF1, 3, 4, 5)-associated [16] and PRR5-, PRR7-, and/or PRR9-associated [15] loci
46 revealed an overlap of 1,460 genes between PIF-bound genes (57.5 % of all PIF-bound
47 genes) and at least one of the three PRRs examined (“PIF-PRR genes”) (Figure 1A left;
48 Dataset 1). The overlap between PIF-bound and PRR5-, PRR7-, or PRR9-bound, when
49 examined individually or in combination, is shown in Figure 1A middle (Dataset 1).
50 Distance between PRR and PIF binding sites indicate that PRRs and PIFs associate to the
51 same genomic regions (Figure 1A right), in accordance with results showing enrichment
52 of G-box-containing motifs in PRR-bound regions [15,22]. We detected interaction of
53 PIF3 and PIF4 with PRR5 (PIF4 in accordance to [20]), PRR7 and PRR9 by yeast two-
54 hybrid assays (Figure S1A). We further confirmed PIF3-PRR interaction *in planta* by
55 BiFc assays (Figure 1B). These data suggest that, similarly to recent findings for TOC1
56 and PIF3 and PIF4 [5,20], PIFs and PRRs may bind together at G-boxes to co-regulate
57 the expression of shared PIF-PRR target genes. Based on the described activity of PRRs
58 as transcriptional repressors [11,12,20], PIF-PRR interaction also agrees with the
59 possibility that PRR5/7/9 might target PIFs to repress their ability to activate shared PIF-
60 PRR target genes as shown recently for TOC1 and PIFs [5,20].

61 Functional classification indicated that “PIF-PRR” genes are enriched in growth-related
62 categories (Figure S1B) and are overrepresented at the elongation phases 18-23
63 specifically under SD (Figure 1C, Figure S1C) (Dataset 1), suggesting that PIFs and
64 PRRs jointly target genes involved in the induction of growth under SD conditions. We
65 compared PRR- and PIF-bound genes with the recently defined PIF- and SD-induced
66 (PIF/SD-induced) gene set of PIFq-regulated genes under SD containing dawn-phased
67 and growth-related genes [4]. Strikingly, one gene (*CDF5*) was PIF/SD-induced and
68 bound by all PRRs and PIFs (Figure 1D, Dataset 1). Previous ChIP experiments showed
69 binding of PRR5/7/9 and possibly TOC1 to this G-box/PBE containing region [15,22,23]
70 (Figure 1E, see legend for details). This region coincides with conserved noncoding
71 sequences (CNS) among crucifer regulatory regions (Figure 1E) [24], suggesting that the
72 binding sites on the *CDF5* promoter have been subjected to selective constraint,
73 consistent with functionality relevance.

74 We verified binding of PRR7, TOC1, PIF3 and PIF4 to the *CDF5* promoter (*pCDF5*)
75 region encompassing the G-boxes at different times under SD conditions by time-course
76 analysis using ChIP-qPCR. Statistically significant and robust PRR7 binding to *pCDF5*
77 was observed at ZT8 and ZT14, and was substantially decreased at ZT24, whereas
78 maximum of TOC1 binding was at ZT14 (Figure 2A). For PIF3 and PIF4, tagged lines
79 driven by the endogenous PIF3 promoter and 35S were used, respectively [25,26] (Figure
80 S2A). Statistically significant binding of PIF3 to *pCDF5* was detected at ZT24, whereas
81 significant PIF4 binding was detected in all three time points and incremented along the
82 night (Figure 2A). These binding dynamics are consistent with the pattern of
83 accumulation of each protein in SD [5,8,27]. Together, these data are consistent with
84 binding of the PIFs, PRRs and TOC1 proteins in SD to the same region of the *CDF5*
85 promoter located approximately 1000 bp upstream of the TSS, and with binding dictated
86 by their protein abundance.

87 To examine how PIF and PRR7 interaction (Figures 1B and S1A) and binding to the
88 *CDF5* promoter (Figure 2A) affect *CDF5* expression, we first tested *CDF5* expression in
89 *pif* and *prr7* mutants under SD at ZT9 when PRR7 levels are maximum and PIFs start to
90 accumulate [7,8,10,27,28]. *CDF5* levels were upregulated in *prr7* (Figure 2B), an effect
91 strongly suppressed by the *pif* mutations in the *prr7pif* double mutants (Figure 2B),
92 suggesting that PIFs and PRR7 regulate *CDF5* expression antagonistically as
93 transcriptional activator and repressor, respectively. Interestingly, because PIF3 transcript
94 and protein levels are not affected in *prr7* (Figures 2C and 2D), together these data
95 suggest that, as described for TOC1 [5], PRR7 acts directly as transcriptional repressor of
96 PIF3 activity in the regulation of *CDF5*. In agreement, the *prr7* long hypocotyl
97 phenotype was also partially suppressed with genetic removal of PIF3 (Figure 2E).
98 However, because the detected binding of PIF3 to the *CDF5* promoter at ZT9 or ZT14
99 was not statistically significant (Figure 2A), we cannot discard that the effect of PRRs on
100 PIF3 might involve inhibition of PIF3 binding to *CDF5* promoter. Suppression of
101 hypocotyl phenotype was also observed for *prr7pif4* and *prr7pif5* compared to *prr7*
102 (Figures 2B and 2E), which suggests that PRR7 directly represses PIF4 transcriptional
103 activity, as previously shown for TOC1 and PIF4 [20], and might also repress PIF5. This
104 scenario might be potentially more complex given that *PIF4/5* transcription is regulated

105 by the clock under SD [2] and at least *PIF4* transcript levels are slightly higher in *prp7*
106 (Figure 2C), in accordance with recent data showing *PIF4* de-repression in *prp* multiple
107 mutants [29]. However, the observation that *CDF5* expression in overexpressing PIF4-
108 HA lines at ZT8 was similar to *pif4* (Figure 2B), a time point where both PRR7 and PIF4
109 are co-bound to the *pCDF5* (Figure 2A), provides strong support that PRR7 directly
110 suppresses PIF4 transcriptional activation activity towards *CDF5*.

111 We next examined the antagonistic PIF-PRR interaction in the direct regulation of *CDF5*
112 across the diurnal cycle. Under SD, phytochrome imposes oscillation of PIF3 and
113 probably PIF1 proteins to progressively accumulate during the night, and to degrade
114 rapidly in the morning maintaining residual levels during the day [8,9]. For PIF4 and
115 possibly PIF5, clock and light regulation result in PIF accumulation also during daytime
116 (Figure 2C) [7,10]. In contrast, PRR accumulation is sequential (PRR9/7/5/TOC1) from
117 morning to midnight (Figure 3A) [21,27]. We therefore expected *CDF5* to oscillate with
118 a peak in the early morning and at the end of the night (where presence of the PIFs is
119 maximum) and a trough from morning to midnight (when PRRs accumulate). Indeed,
120 *CDF5* in the WT was detected during the first part of the day (ZT0-ZT3), then declined
121 to almost undetectable levels through ZT15, and accumulated after ZT15 to peak at dawn
122 (Figure 3B). Expression in *pifq* SD and in WT LL at dawn (a condition where PIFs do not
123 accumulate) [28] was lower than WT SD (Figure 3B), supporting the notion that
124 transcript induction leading to the oscillatory pattern of *CDF5* expression in SD depends
125 on the presence of the PIFs (Figure 3B). Analysis of *CDF5* levels in single *pif* and
126 multiple *pifq* (defective in PIF1/3/4/5) mutants at ZT24 showed that the PIF quartet
127 (PIFq) collectively induces *CDF5* expression at dawn, with PIF1 having a lesser
128 contribution (Figure 3C). *CDF5* transcript levels dropped in the WT after 1h of morning
129 light (Figure 3B), concurrent with phy-induced PIF degradation. In contrast, at ZT9,
130 when *CDF5* expression in the WT is almost non-detectable, *CDF5* expression was
131 significantly higher in *prp5*, *prp7*, *prp79*, *prp59*, and *prp579*, with a major contribution for
132 PRR7 (Figure S2B). Compared to WT, *CDF5* expression was higher in *prp7* from ZT3
133 through midnight (Figure 3D), whereas in *prp59* and *prp79* mutants *CDF5* expression
134 was only slightly higher at dawn in *prp59* and higher from dusk to dawn in *prp79* (Figure
135 3D). In *toc1*, de-repression of *CDF5* was early compared to WT (Figure S2C), similar to

136 other PIF-TOC1 co-targets [5]. Because cross-regulation was described in the PRRs [30],
137 with nuclear accumulation of TOC1 depending partly on PRR5, it is likely that TOC1
138 contributes to the phenotype of PRR5-deficient mutant backgrounds. We also
139 characterized *PRR5* and *PRR7* expression in *prp79* and *prp59* double mutants,
140 respectively. Levels of *PRR5* and *PRR7* were ~1.5-fold higher in *prp59* and *prp79*
141 compared to WT, and *PRR5* phase was delayed in *prp79*, indicative of intricate cross-
142 regulatory pathways (Figure S2D). Significantly, *CDF5* expression in the *prp59* mutant
143 from ZT3-ZT21 was almost linear (Figure 3D), in accordance with the PRRs (with TOC1
144 possibly also contributing) being responsible for the repression of *CDF5* expression from
145 morning to midnight.

146 To further examine the PIF-PRR antagonistic interplay, we artificially induced PIF
147 accumulation at the beginning of the night period when PRR levels are high (Figure 3A)
148 [27] by giving a far-red light pulse (FRp) at ZT8 [5,28]. As control we used *PIL1*, a direct
149 PIF target and marker gene for PIF abundance and activity [8]. *PIL1* levels accumulated
150 in the WT immediately after the FRp (Figure 3E), in agreement with the rapid
151 accumulation of PIF proteins after a FRp [9,25,31], and to PRRs not interfering
152 significantly with PIF activity in the regulation of *PIL1*, in accordance with *PIL1* not
153 being a direct target of all PRRs [15]. In striking contrast, expression induction of the
154 PIF-PRR target *CDF5* was repressed in the WT during the first part of the night (ZT8-
155 ZT16) after a FRp, similarly to the control (-FRp) samples (Figure 3E). Interestingly, this
156 repression was much lower in *prp5* and *prp7*, and not observed in *prp59*. In *toc1*, early
157 *CDF5* expression compared to WT (Figures 3E and S2C) was more evident in (+FRp)
158 samples.

159 Although part of the effect seen in *prp* mutants might come from elevated PIF4/5 levels
160 due to their transcriptional derepression (Fig 2C), together these data support the
161 conclusion that the PRR9/7/5 and TOC1 prevent the transcriptional activation of *CDF5*
162 by PIFs. Given the sequential pattern of expression of *PRR9*, *7*, *5*, and *TOC1* (Figure 3A)
163 [21], and the progressive accumulation of the PIFs along the night in SD conditions [8],
164 our findings suggest that *CDF5* is sequentially targeted by *PRR9*, *7*, *5*, and *TOC1* to
165 repress its expression from morning to midnight (when PRR and TOC1 levels are high),
166 to gate PIF direct induction of *CDF5* to dawn when the levels of PRRs and TOC1 are low

167 and PIFs reach a peak in abundance. We propose that *CDF5* might be a novel target of
168 this PRR and PIF interplay in the promotion of hypocotyl elongation.

169 Our findings suggest a model where the antagonistic regulation of *CDF5* gene expression
170 by PRRs and PIFs described above might underlie rhythmic growth under SD. In
171 agreement, we observed correlation between the magnitude of hypocotyl length under our
172 SD conditions and *CDF5* levels in *prp* and *pifq* mutants (Figures S3A and S3B). To test
173 this model genetically, we generated seedlings ectopically expressing *CDF5* in a *cdf5*
174 mutant background (*CDF5OX*) (Figure S3C), and quantified the hypocotyl phenotype of
175 WT, *CDF5OX*, and *cdf5* lines under SD. *cdf5* mutants were slightly shorter than WT SD-
176 grown seedlings, whereas *CDF5OX* lines suppressed the *cdf5* phenotype and showed a
177 range from subtle to robustly elongated hypocotyls compared to WT (Figures 4A). We
178 analyzed the elongation rate of *cdf5* and *CDF5OX* lines under SD compared to WT
179 (Figure 4B). As described, the growth rate of WT seedlings is highest during the second
180 half of the night [2]. Elongation rate of *cdf5* seedlings was similar to WT during the day
181 and first part of the night, but it was reduced during the last part of the night, when *CDF5*
182 expression in the WT is maximum, consistent with their short phenotype. Interestingly,
183 elongation rate of *CDF5OX* seedlings was constantly high during the day and most part
184 of the night (Figure 4B). Together, our data suggest that transcriptional control of *CDF5*
185 expression by the PIFs and PRRs is a key regulatory mechanism in growth control.

186 Next, to genetically test the interplay between *CDF5*, PIFs and PRRs, we generated
187 *prp7cdf5*, *pifqcdf5* and *pifqCDF5OX* and mutants (Figure S3C) to study their hypocotyl
188 phenotypes. We observed that in SD the quintuple *pifqcdf5* mutant displayed a phenotype
189 similar to *pifq*, indicating that the *cdf5* mutation did not have an additive effect on *pifq*
190 mutation (Figure 4A). This result agrees with PIFq and *CDF5* acting in the same
191 signaling pathway. Overexpression of *CDF5* in the *pifq* background partially restored the
192 *pifq* phenotype (Figures 4A), providing additional evidence that *CDF5* contributes to
193 growth downstream of the PIFs. Finally, comparison of *prp7* with *prp7cdf5* mutants
194 showed that the long phenotype of *prp7* under SD is reduced when *CDF5* is removed in
195 *prp7cdf5* (Figures 4A), suggesting that exaggerated growth in *prp7* is partially a
196 consequence of having elevated levels of *CDF5*. Together, our results confirm our model

197 where PRRs and PIFs directly and antagonistically regulate *CDF5* expression to precisely
198 gate *CDF5* growth-promoting activity to the end of the night.

199 We hypothesized that *CDF5* might control the expression of growth-related genes at
200 dawn downstream of PIFq. We selected a few PIF-regulated [4], growth-related cell wall
201 [32] and SD growth-marker genes [6,8] to test for their expression in *cdf5* and *CDF5OX*
202 lines. As shown in Figure 4C, *PIL1* and *XTR7* were not significantly affected in *cdf5* or
203 *CDF5OX*, and *IAA19*, *YUCCA8* and three selected cell wall related genes (*AGP4*, *PME*,
204 and *FLA9*) show either significant down-regulation in *cdf5* (*IAA19*), up-regulation in
205 *CDF5OX* (*PME*, *AGP4*), or both (*YUC8* and *FLA9*), compared to the WT. Interestingly,
206 *AGP4* and *PME* are not PIF-bound genes. These results suggest branching downstream of
207 PIFq, with *CDF5* regulating a subset of the PIFq-regulated growth-related genes, in
208 accordance to the partial suppression of the *pifq* phenotype by *CDF5OX* shown above
209 (Figure 4A). Examination of the hypocotyl cell size in SD-grown WT, *cdf5* and *CDF5OX*
210 seedlings by confocal microscopy imaging clearly showed elongated cells in *CDF5OX*
211 hypocotyls compared to WT, whereas cells in *cdf5* appeared shorter (Figure 4D left),
212 which was confirmed by quantification of the hypocotyl cell length (Figure 4D right).
213 Next, we tested *prp7*, which exhibited a longer cell phenotype partially suppressed by
214 genetic removal of *CDF5* in *prp7cdf5* (Figure 4D). In contrast, cell length in *pifq* was
215 shorter than WT, a phenotype that was partially recovered by *CDF5OX* (Figure 4C right).
216 Together, these results support a role for *CDF5* in the promotion of cell elongation under
217 the inductive growth condition of SDs downstream of PRRs and PIFs.

218 **Conclusions**

219 Here we found that members of the PRR family of transcriptional repressors (PRR5, 7,
220 and 9), with a key role in the regulation of the central circadian oscillator and clock
221 output processes in plants [12], target growth-related genes that are directly induced by
222 the growth-promoting PIF transcription factors. Given the coincident DNA-binding
223 specificity of PRRs and PIFs (Figure 1A) [15,33], the PIF-PRR physical interaction in the
224 nucleus (Figures 1B and S1A), and their accumulation dynamics during short-day
225 photoperiods (Figure 3A) [2,7,8,11,21], we propose a model in which successive binding
226 of the PRR9, PRR7, and PRR5 to the G-box elements of shared PIF and PRR target
227 genes (like the growth-promoting *CDF5*) acts to sequentially repress transcription of the

228 PIF-induced transcriptional network starting in the morning (Figure 4E, Figure S4).
229 Given that PRR9/7/5 have not been shown to bind DNA directly, our results agree with
230 the possibility that PIFs might bridge the binding of PRRs to DNA, although competition
231 by direct binding of PRR to G-boxes, or through a PRR- and G-box- binding factor
232 different than PIFq, cannot be completely discarded based on our results. These findings
233 define an expanded framework for previous results showing PRR1/TOC1 repression of
234 PIF transcriptional activity at midnight [5]. At dawn, PRRs and TOC1 are not present,
235 PIF protein accumulation reaches a maximum, and elongation is promoted by PIF-
236 induced expression of growth-promoting genes like *CDF5* (Figure 4E). Collectively, our
237 data reveal that gating of growth occurs not only at the post-dusk hours of the night as
238 previously described for TOC1 [5], but instead starts in the morning and covers all the
239 day period until midnight through the sequential action of the PRR family of
240 transcriptional repressors. The molecular mechanism described here could explain why
241 growth rate under short-day photoperiods is low [2] from morning to midnight in the
242 presence of low PIF3 and PIF1 [9,34] and considerable high amounts of PIF4 (and likely
243 PIF5) [7,10], a regulation critical for fitness by preventing overgrowth (Figure 4A). Our
244 results reveal that gating of growth has evolved in plants to encompass the orchestrated
245 sequential action of members of the PRR family (PRR9/7/5/1) of transcriptional
246 repressors that peak in waves from morning to midnight. This function highlights the dual
247 role of the PRR family of clock oscillator components, as regulators of central clock
248 components and cycling outputs [11,21,35], and as repressors of the physiological output
249 of growth in combined regulation with light pathways that control accumulation of PIFs.

250 **Acknowledgements**

251 We thank D. Somers, S.Pratt, G. Coupland, and R. McClung for sharing seed and plasmid
252 resources. We thank G. Steele for generating double and triple *prp* mutants, and the *prp*
253 mutant combinations. The work in this manuscript was supported by grants from the
254 Spanish “Ministerio de Economía y Competitividad” (MINECO) BIO2012-31672 and
255 BIO2015-68460-P, and from the Generalitat de Catalunya 2014-SGR-1406 to E.M.; by
256 Marie Curie IRG PIRG06-GA-2009-256420 grant to P.L.; by the European Commission
257 (PCIG2012-GA-2012-334052) and by MINECO (BIO2015-70812-ERC; RYC-2011-

258 09220) to R.H.; by Royal Society Grant RG2016R1 to G. T-O; by MINECO BIO2013-
259 43184-P to D.A; by MINECO AGL2014-57200-JIN to E.G.M. We acknowledge
260 financial support by the CERCA programme/Generalitat de Catalunya and from
261 MINECO through the “Severo Ochoa Programme for Centers of Excellence in R&D”
262 2016-2019 (SEV-2015-0533)”.

263 **Author contributions**

264 G.M., P.L., and E.M. conceived and designed the study, G.M., A.R., N.V., J.S., G.T-O.,
265 C.M.M.G., M.B., R.H., E.G.M., D.A., K.H., P.L., and E.M. acquired, analyzed and
266 interpreted data. G.M., P.L., and E.M. wrote the manuscript.

267 **Declaration of Interests**

268 The authors declare no competing interests.

269 **References**

- 270 1. Niwa, Y., Yamashino, T., and Mizuno, T. (2009). The Circadian Clock Regulates
271 the Photoperiodic Response of Hypocotyl Elongation through a Coincidence
272 Mechanism in *Arabidopsis thaliana*. *Plant Cell Physiol.* *50*, 838–854.
- 273 2. Nozue, K., Covington, M.F., Duek, P.D., Lorrain, S., Fankhauser, C., Harmer,
274 S.L., and Maloof, J.N. (2007). Rhythmic growth explained by coincidence
275 between internal and external cues. *Nature* *448*, 358–361.
- 276 3. Nomoto, Y., Kubozono, S., Yamashino, T., Nakamichi, N., and Mizuno, T. (2012).
277 Circadian Clock- and PIF4-Controlled Plant Growth: A Coincidence Mechanism
278 Directly Integrates a Hormone Signaling Network into the Photoperiodic Control
279 of Plant Architectures in *Arabidopsis thaliana*. *Plant Cell Physiol.* *53*, 1950–1964.
- 280 4. Martín, G., Soy, J., and Monte, E. (2016). Genomic Analysis Reveals Contrasting
281 PIFq Contribution to Diurnal Rhythmic Gene Expression in PIF-Induced and -
282 Repressed Genes. *Front. Plant Sci.* *7*, 962.
- 283 5. Soy, J., Leivar, P., González-Schain, N., Martín, G., Diaz, C., Sentandreu, M., Al-
284 Sady, B., Quail, P.H., and Monte, E. (2016). Molecular convergence of clock and
285 photosensory pathways through PIF3–TOC1 interaction and co-occupancy of
286 target promoters. *Proc. Natl. Acad. Sci. U. S. A.* *113*, 4870–4875.
- 287 6. Nozue, K., Harmer, S.L., and Maloof, J.N. (2011). Genomic Analysis of Circadian
288 Clock-, Light-, and Growth-Correlated Genes Reveals PHYTOCHROME-
289 INTERACTING FACTOR5 as a Modulator of Auxin Signaling in *Arabidopsis*.

- 290 Plant Physiol. *156*, 357–372.
- 291 7. Bernardo-García, S., de Lucas, M., Martínez, C., Espinosa-Ruiz, A., Davière, J.-
292 M., and Prat, S. (2014). BR-dependent phosphorylation modulates PIF4
293 transcriptional activity and shapes diurnal hypocotyl growth. *Genes Dev.* *28*,
294 1681–1694.
- 295 8. Soy, J., Leivar, P., González-Schain, N., Sentandreu, M., Prat, S., Quail, P.H., and
296 Monte, E. (2012). Phytochrome-imposed oscillations in PIF3 protein abundance
297 regulate hypocotyl growth under diurnal light/dark conditions in *Arabidopsis*.
298 *Plant J.* *71*, 390–401.
- 299 9. Monte, E., Tepperman, J.M., Al-Sady, B., Kaczorowski, K.A., Alonso, J.M.,
300 Ecker, J.R., Li, X., Zhang, Y., and Quail, P.H. (2004). The phytochrome-
301 interacting transcription factor, PIF3, acts early, selectively, and positively in light-
302 induced chloroplast development. *Proc. Natl. Acad. Sci. U. S. A.* *101*, 16091–
303 16098.
- 304 10. Yamashino, T., Nomoto, Y., Lorrain, S., Miyachi, M., Ito, S., Nakamichi, N.,
305 Fankhauser, C., and Mizuno, T. (2013). Verification at the protein level of the
306 PIF4-mediated external coincidence model for the temperature-adaptive
307 photoperiodic control of plant growth in *Arabidopsis thaliana*. *Plant Signal. Behav.*
308 *8*, e23390.
- 309 11. Nakamichi, N., Kiba, T., Henriques, R., Mizuno, T., Chua, N.-H., and Sakakibara,
310 H. (2010). PSEUDO-RESPONSE REGULATORS 9, 7, and 5 Are Transcriptional
311 Repressors in the *Arabidopsis* Circadian Clock. *Plant Cell* *22*, 594–605.
- 312 12. Farré, E.M., and Liu, T. (2013). The PRR family of transcriptional regulators
313 reflects the complexity and evolution of plant circadian clocks. *Curr. Opin. Plant*
314 *Biol.* *16*, 621–629.
- 315 13. Nakamichi, N., Kita, M., Ito, S., Yamashino, T., and Mizuno, T. (2005).
316 PSEUDO-RESPONSE REGULATORS, PRR9, PRR7 and PRR5, Together Play
317 Essential Roles Close to the Circadian Clock of *Arabidopsis thaliana*. *Plant Cell*
318 *Physiol.* *46*, 686–698.
- 319 14. Kaczorowski, K.A., and Quail, P.H. (2003). *Arabidopsis* PSEUDO-RESPONSE
320 REGULATOR7 Is a Signaling Intermediate in Phytochrome-Regulated Seedling
321 Deetiolation and Phasing of the Circadian Clock. *Plant Cell* *15*, 2654–2665.
- 322 15. Liu, T.L., Newton, L., Liu, M.-J., Shiu, S.-H., and Farré, E.M. (2016). A G-Box-
323 Like Motif Is Necessary for Transcriptional Regulation by Circadian Pseudo-
324 Response Regulators in *Arabidopsis*. *Plant Physiol.* *170*, 528–539.
- 325 16. Pfeiffer, A., Shi, H., Tepperman, J.M., Zhang, Y., and Quail, P.H. (2014).
326 Combinatorial Complexity in a Transcriptionally Centered Signaling Hub in
327 *Arabidopsis*. *Mol. Plant* *7*, 1598–1618.

- 328 17. Martínez-García, J.F., Huq, E., and Quail, P.H. (2000). Direct Targeting of Light
329 Signals to a Promoter Element-Bound Transcription Factor. *Science* 288, 859–863.
- 330 18. Fornara, F., de Montaigu, A., Sánchez- Villarreal, A., Takahashi, Y., Ver Loren
331 van Themaat, E., Huettel, B., Davis, S.J., and Coupland, G. (2015). The GI–CDF
332 module of Arabidopsis affects freezing tolerance and growth as well as flowering.
333 *Plant J.* 81, 695–706.
- 334 19. Fornara, F., Panigrahi, K.C.S., Gissot, L., Sauerbrunn, N., Rühl, M., Jarillo, J.A.,
335 and Coupland, G. (2009). Arabidopsis DOF Transcription Factors Act
336 Redundantly to Reduce CONSTANS Expression and Are Essential for a
337 Photoperiodic Flowering Response. *Dev. Cell* 17, 75–86.
- 338 20. Zhu, J.-Y., Oh, E., Wang, T., and Wang, Z.-Y. (2016). TOC1–PIF4 interaction
339 mediates the circadian gating of thermoresponsive growth in Arabidopsis. *Nat.*
340 *Commun.* 7, 13692.
- 341 21. Matsushika, A., Makino, S., Kojima, M., and Mizuno, T. (2000). Circadian Waves
342 of Expression of the APRR1/TOC1 Family of Pseudo-Response Regulators in
343 Arabidopsis thaliana: Insight into the Plant Circadian Clock. *Plant Cell Physiol.*
344 41, 1002–1012.
- 345 22. Nakamichi, N., Kiba, T., Kamioka, M., Suzuki, T., Yamashino, T., Higashiyama,
346 T., Sakakibara, H., and Mizuno, T. (2012). Transcriptional repressor PRR5 directly
347 regulates clock-output pathways. *Proc. Natl. Acad. Sci. U. S. A.* 109, 17123–
348 17128.
- 349 23. Huang, W., Pérez-García, P., Pokhilko, A., Millar, A.J., Antoshechkin, I.,
350 Riechmann, J.L., and Mas, P. (2012). Mapping the Core of the Arabidopsis
351 Circadian Clock Defines the Network Structure of the Oscillator. *Science* 336, 75–
352 79.
- 353 24. Haudry, A., Platts, A.E., Vello, E., Hoen, D.R., Leclercq, M., Williamson, R.J.,
354 Forczek, E., Joly-Lopez, Z., Steffen, J.G., Hazzouri, K.M., *et al.* (2013). An atlas
355 of over 90,000 conserved noncoding sequences provides insight into crucifer
356 regulatory regions. *Nat Genet* 45, 891–898.
- 357 25. Lorrain, S., Allen, T., Duek, P.D., Whitelam, G.C., and Fankhauser, C. (2008).
358 Phytochrome-mediated inhibition of shade avoidance involves degradation of
359 growth-promoting bHLH transcription factors. *Plant J.* 53, 312–323.
- 360 26. Al-Sady, B., Ni, W., Kircher, S., Schäfer, E., and Quail, P.H. (2006).
361 Photoactivated Phytochrome Induces Rapid PIF3 Phosphorylation Prior to
362 Proteasome-Mediated Degradation. *Mol. Cell* 23, 439–446.
- 363 27. Fujiwara, S., Wang, L., Han, L., Suh, S.-S., Salomé, P.A., McClung, C.R., and
364 Somers, D.E. (2008). Post-translational Regulation of the Arabidopsis Circadian
365 Clock through Selective Proteolysis and Phosphorylation of Pseudo-response

- 366 Regulator Proteins. *J. Biol. Chem.* 283, 23073–23083.
- 367 28. Soy, J., Leivar, P., and Monte, E. (2014). PIF1 promotes phytochrome-regulated
368 growth under photoperiodic conditions in *Arabidopsis* together with PIF3, PIF4,
369 and PIF5. *J. Exp. Bot.* 65, 2925–2936.
- 370 29. Hayama, R., Sarid- Krebs, L., Richter, R., Fernández, V., Jang, S., and Coupland,
371 G. (2017). PSEUDO RESPONSE REGULATORS stabilize CONSTANS protein
372 to promote flowering in response to day length. *EMBO J.* 36, 904–918.
- 373 30. Wang, L., Fujiwara, S., and Somers, D.E. (2010). PRR5 regulates phosphorylation,
374 nuclear import and subnuclear localization of TOC1 in the *Arabidopsis* circadian
375 clock. *EMBO J.* 29, 1903–1915.
- 376 31. Shen, H., Moon, J., and Huq, E. (2005). PIF1 is regulated by light-mediated
377 degradation through the ubiquitin-26S proteasome pathway to optimize
378 photomorphogenesis of seedlings in *Arabidopsis*. *Plant J.* 44, 1023–1035.
- 379 32. Pelletier, S., Van Orden, J., Wolf, S., Vissenberg, K., Delacourt, J., Ndong, Y.A.,
380 Pelloux, J., Bischoff, V., Urbain, A., Mouille, G., *et al.* (2010). A role for pectin
381 de-methylesterification in a developmentally regulated growth acceleration in
382 dark-grown *Arabidopsis* hypocotyls. *New Phytol.* 188, 726–739.
- 383 33. Heyndrickx, K.S., de Velde, J. Van, Wang, C., Weigel, D., and Vandepoele, K.
384 (2014). A Functional and Evolutionary Perspective on Transcription Factor
385 Binding in *Arabidopsis thaliana*. *Plant Cell* 26, 3894-3910.
- 386 34. Huq, E., Al-Sady, B., Hudson, M., Kim, C., Apel, K., and Quail, P.H. (2004).
387 PHYTOCHROME-INTERACTING FACTOR 1 Is a Critical bHLH Regulator of
388 Chlorophyll Biosynthesis. *Science* 305, 1937–1941.
- 389 35. Kamioka, M., Takao, S., Suzuki, T., Taki, K., Higashiyama, T., Kinoshita, T., and
390 Nakamichi, N. (2016). Direct Repression of Evening Genes by CIRCADIAN
391 CLOCK-ASSOCIATED1 in the *Arabidopsis* Circadian Clock. *Plant Cell* 28, 696–
392 711.
- 393 36. Kikis, E.A., Khanna, R., and Quail, P.H. (2005). ELF4 is a phytochrome-regulated
394 component of a negative-feedback loop involving the central oscillator
395 components CCA1 and LHY. *Plant J.* 44, 300–313.
- 396 37. Leivar, P., Monte, E., Oka, Y., Liu, T., Carle, C., Castillon, A., Huq, E., and Quail,
397 P.H. (2008). Multiple Phytochrome-Interacting bHLH Transcription Factors
398 Repress Premature Seedling Photomorphogenesis in Darkness. *Curr. Biol.* 18,
399 1815–1823.
- 400 38. Khanna, R., Shen, Y., Marion, C.M., Tsuchisaka, A., Theologis, A., Schäfer, E.,
401 and Quail, P.H. (2008). The Basic Helix-Loop-Helix Transcription Factor PIF5
402 Acts on Ethylene Biosynthesis and Phytochrome Signaling by Distinct

- 403 Mechanisms. *Plant Cell* 19, 3915-3929.
- 404 39. Michael, T.P., Salomé, P.A., Yu, H.J., Spencer, T.R., Sharp, E.L., McPeck, M.A.,
405 Alonso, J.M., Ecker, J.R., and McClung, C.R. (2003). Enhanced Fitness Conferred
406 by Naturally Occurring Variation in the Circadian Clock. *Science* 302, 1049–1053.
- 407 40. Fujimori, T., Yamashino, T., Kato, T., and Mizuno, T. (2004). Circadian-
408 Controlled Basic/Helix-Loop-Helix Factor, PIL6, Implicated in Light-Signal
409 Transduction in *Arabidopsis thaliana*. *Plant Cell Physiol.* 45, 1078–1086.
- 410 41. Más, P., Alabadí, D., Yanovsky, M.J., Oyama, T., and Kay, S.A. (2003). Dual
411 Role of TOC1 in the Control of Circadian and Photomorphogenic Responses in
412 *Arabidopsis*. *Plant Cell* 15, 223–236.
- 413 42. Liu, T., Carlsson, J., Takeuchi, T., Newton, L., and Farré, E.M. (2013). Direct
414 regulation of abiotic responses by the *Arabidopsis* circadian clock component
415 PRR7. *Plant J.* 76, 101–114.
- 416 43. Nicol, J.W., Helt, G.A., Blanchard Steven G., J., Raja, A., and Loraine, A.E.
417 (2009). The Integrated Genome Browser: free software for distribution and
418 exploration of genome-scale datasets. *Bioinformatics* 25, 2730–2731.
- 419 44. Huang, D.W., Sherman, B.T., Tan, Q., Collins, J.R., Alvord, W.G., Roayaei, J.,
420 Stephens, R., Baseler, M.W., Lane, H.C., and Lempicki, R.A. (2007). The DAVID
421 Gene Functional Classification Tool: a novel biological module-centric algorithm
422 to functionally analyze large gene lists. *Genome Biol.* 8, R183.
- 423 45. Toledo-Ortiz, G., Johansson, H., Lee, K.P., Bou-Torrent, J., Stewart, K., Steel, G.,
424 Rodríguez-Concepción, M., and Halliday, K.J. (2014). The HY5-PIF Regulatory
425 Module Coordinates Light and Temperature Control of Photosynthetic Gene
426 Transcription. *PLoS Genet.* 10, e1004416.
- 427 46. Ni, M., Tepperman, J.M., and Quail, P.H. (1998). PIF3, a Phytochrome-Interacting
428 Factor Necessary for Normal Photoinduced Signal Transduction, Is a Novel Basic
429 Helix-Loop-Helix Protein. *Cell* 95, 657–667.
- 430 47. Wang, L., Kim, J., and Somers, D.E. (2013). Transcriptional corepressor
431 TOPLESS complexes with pseudoresponse regulator proteins and histone
432 deacetylases to regulate circadian transcription. *Proc. Natl. Acad. Sci. U. S. A.*
433 110, 761–766.
- 434 48. Tanaka, Y., Kimura, T., Hikino, K., Goto, S., Nishimura, M., Mano, S., and
435 Nakagawa, T. (2012). Gateway Vectors for Plant Genetic Engineering: Overview
436 of Plant Vectors, Application for Bimolecular Fluorescence Complementation
437 (BiFC) and Multigene Construction. *InTech*.
- 438 49. Martín, G., Leivar, P., Ludevid, D., Tepperman, J.M., Quail, P.H., and Monte, E.
439 (2016). Phytochrome and retrograde signalling pathways converge to

440 antagonistically regulate a light-induced transcriptional network. Nat. Commun. 7,
441 11431.

442

443

444 **Figure Legends**

445 **Figure 1. Analysis of coincident co-binding of PRRs and PIFs to dawn-phased genes**
446 **under SD identifies *CDF5* as a PIF- and PRR5/7/9-bound gene.** (A) (Left)
447 Comparison of PIF-bound [16] and PRR5-, 7- and/or PRR9-bound genes [15] (gene lists
448 provided in Dataset 1) defines three groups of genes: “PIF only” (1,384 genes), “PRR
449 only” (3,013 genes), and “PIF-PRR” (1,460 genes). (Middle) Percentage of PIF-bound
450 genes in genes bound by single or a combination of PRRs. (Right) Frequency of pairwise
451 distance in base pairs (bp) between the PIF- and PRR- binding sites in each of the “PIF-
452 PRR” co-bound genes. (B) BiFC assay of the PRRs and PIF3 fusions to N- and C-
453 terminal fragments of YFP, respectively, in transfected onion cells. The combinations of
454 PIF3-cYFP and TOC1-nYFP or pGW-nYFP were used as positive and negative control,
455 respectively. (Left) YFP fluorescence image. (Center) Bright-field image. (Right) Merge
456 of YFP fluorescence and bright-field image. (C) Expression phases in SD of gene sets
457 defined in (A): “PIF-PRR” (purple), “PRR only” (pink), and “PIF only” (yellow). Phases
458 are indicated on the circumference, and fold-change phase enrichment of genes
459 (count/expected) on the radius. Day is shown in yellow; night in gray. See also Figure
460 S1 and Dataset 1. (D) Comparison of PIF- [16], PRR5-, 7-, and PRR9-bound genes [15],
461 and “PIF/SD-induced” genes [4] (see Dataset 1 for details) (E) Visualization of ChIP-seq
462 and ChIP-qPCR data in the genomic region encompassing the *CDF5* locus co-bound by
463 PIFs, PRRs and TOC1. For PIF (orange), ChIP-seq tracks show the pile-up of all the
464 reads obtained from MACS analyses (model based for ChIP-seq) of the dataset from
465 each experiment [16]. Each corresponding WT-ChIP/input control is overlaid in dark
466 gray. For PRR (purple), filled rectangles indicate the PRR9, PRR7 and PRR5 peaks
467 defined by ChIP-seq in [15]. Empty rectangles indicate peaks only described by ChIP-
468 qPCR, in [22] for PRR9 and in Figure 2A for TOC1. Conserved non-coding sequences
469 (CNS) (blue) are defined in [24]. G- and PBE-box: vertical lines indicate motif positions.
470 See also Figure S1 and Dataset 1.

471 **Figure 2. PRR7 represses PIF3 ability to induce *CDF5* expression in SD.** (A) PRR7,
472 TOC1, PIF3, and PIF4 binding to the G-box containing region of the *CDF5* promoter at
473 ZT8, ZT14, and ZT24 under SD. For ChIP-qPCR analysis, samples of SD-grown
474 *pPRR7::PRR7-GFP* (PRR7-GFP), *pTOC1::TOC1:YFP* (TMG), *pPIF3::YFP:PIF3*

475 (YFP-PIF3), and *35S::PIF4-HA* (PIF4-HA), were harvested at the indicated times during
476 the third day and were immunoprecipitated using anti-GFP or anti-HA antibodies. Data
477 are from three independent ChIP experiments, and error bars indicate SE. Statistically
478 significant differences between mean values by Student's *t*-test relative to WT are shown
479 ($*P<0.05$; $**P<0.01$ and $***P<0.001$). n.s., not significant. WT controls were Col-0 for
480 YFP-PIF3, PIF4-HA, and PRR7-GFP, and C24 for TMG seedlings. Ab: samples
481 immunoprecipitated with antibody. No Ab: control samples immunoprecipitated without
482 antibody. (B) *CDF5* expression levels in WT, *pif3*, *pif4*, *pif5*, *prp7*, *prp7pif3*, *prp7pif4*,
483 *prp7pif5*, and PIF4-HA. Samples were harvested at ZT9 during the third day of growth
484 (ZT8 for PIF4-HA), analyzed by qRT-PCR and normalized to *PP2A*. Data are from three
485 independent biological replicates relative to WT set at one. Different letters denote
486 statistically significant differences among means by Tukey-b test ($P<0.05$). Error bars
487 indicate SE. (C) WT and *prp7* seedlings grown for 2 d in SD conditions were harvested
488 during the third day at the indicated times. Expression levels of *PIF3* and *PIF4* were
489 analyzed by qRT-PCR, and values were normalized to *PP2A*. Data plotted are mean \pm SE
490 relative to *PIF4* WT at ZT3 set at one, $n = 2$ independent biological experiments, each
491 assayed in triplicate. (D) PIF3 protein levels in 3-day old SD-grown WT and *prp7*
492 seedlings at ZT24. C-blue, coomassie blue; NS, non-specific bands. (E) Hypocotyl length
493 in seedlings as in (B) (except for PIF4-HA) grown for 3 days in SD. Different letters
494 denote statistically significant differences among means by Tukey-b test ($P<0.05$). Data
495 are means \pm SE of at least 50 seedlings. See also Figure S2.

496 **Figure 3. PRRs and PIFs antagonistically regulate *CDF5* to dawn-phase its**
497 **expression under diurnal SD conditions. (A)** Transcriptional waves of *PRR9/7/5* and
498 *TOC1* expression during the third day in SD at the indicated times. Each gene is
499 expressed relative to its maximum expression value set at one. (B-D) *CDF5* expression
500 in WT, *pif*, and *prp* analyzed by qRT-PCR (B) Expression in 2-day-old SD-grown
501 seedlings harvested during the third day at the indicated times in seedlings kept under SD
502 or moved to continuous light (LL). Data are relative to WT SD ZT3. (C) Expression in
503 3-day-old seedlings at ZT24 grown as in (B). Data are from two independent biological
504 replicates and are relative to WT samples set at one. Percentage is the contribution of
505 each PIF to *CDF5* expression in SD considering *pifq* and WT values as 0% and 100%,

506 respectively. Error bars indicate SE. **(D)** Expression in WT, *prp5*, *prp7*, *prp9*, *prp59*,
507 *prp79*, and *prp579* seedlings grown for 2 d in SD conditions during the third day at the
508 indicated times. Expression is relative to *CDF5* WT at ZT3. **(E)** *PIL1* and *CDF5*
509 expression in WT, *prp* and *toc1* analyzed by qRT-PCR. Two-day-old SD-grown
510 seedlings were treated with a 15-min far-red pulse (FRp) at ZT8 on the third day ((+) FRp
511 samples, in red), and harvested during the night at ZT9, ZT12, ZT16 and ZT20. (-) FRp
512 control samples (in black) did not receive a FRp. Data are relative to ZT8 set at one for
513 each genotype. (A-E) All samples were normalized to *PP2A*. (A-B, D-E) Data plotted
514 are mean \pm SE, n=2 independent biological experiments, each assayed in triplicate. See
515 also Figures S2 and S3.

516 **Figure 4. PRR- and PIF-mediated regulation of cell elongation requires CDF5.** **(A)**
517 Hypocotyl length of WT, *cdf5*, *CDF5OX*, *pifq*, *pifqCDF5OX*, *prp7*, and *prp7cdf5* grown
518 for 3 and 4 days in SD (left). Data are means \pm SE of at least 35 seedlings. Different
519 letters denote statistically significant differences among means by Tukey-b test ($P < 0.05$).
520 Visible phenotypes of 3-day-old seedlings are shown in the right. Scale bar = 5 mm. **(B)**
521 Hypocotyl elongation rate for WT, *cdf5* and *CDF5OX 5.7* under SD conditions. Seedling
522 growth was monitored every 2 hours during the third day. Average of 12 seedlings is
523 shown, and SE is indicated by the shaded area. **(C)** Expression of PIF-regulated growth
524 marker genes (top) and cell wall genes (bottom) in 3-day-old SD-grown WT, *cdf5* and
525 *CDF5OX 5.7* seedlings at ZT24, analyzed by qRT-PCR and normalized to *PP2A*. Data
526 are from three independent biological replicates normalized to WT set at one. Error bars
527 indicate SE. Statistically significant differences between mean values by Student's *t*-test
528 relative to WT are shown (* $P < 0.05$; ** $P < 0.01$ and *** $P < 0.001$). n.s., not significant. **(D)**
529 (Left) Visual phenotypes of cell area in 3d-old SD-grown WT, *cdf5* and *CDF5OX 5.7*
530 seedling hypocotyls. Scale bar = 200 μ m. (Right) Quantification of cell length in WT,
531 *cdf5*, *CDF5OX 5.7*, *pifq*, *pifqCDF5OX* (*pifqOX* in the figure), *prp7*, and *prp7cdf5*.
532 Seedlings were grown for 3 days in SD. Data are means \pm SE of at least 100 cells from
533 3-4 independent seedlings. Different letters or an asterisk denote statistically significant
534 differences among means by Tukey-b test ($P < 0.05$) or by *t*-test ($P < 0.05$), respectively.
535 **(E)** Model of the proposed role of PRRs as repressors of PIF activity to regulate cell
536 elongation through *CDF5*. PIFs bind to the *CDF5* promoter and induce *CDF5*

537 transcription in the absence of PRRs. If PRRs are present, PRRs repress PIF
538 transcriptional activity through direct PIF-PRR interaction. Based on current data, PRRs
539 and PIFs could bind to the same or different nearby G-boxes, or alternatively, PRRs
540 could bind indirectly to G-boxes through DNA-bound PIFs or other G-box and PRR-
541 binding factors. Sequential PRR9/7/5 and PRR1/TOC1 accumulation from morning to
542 midnight gate PIF-induction of *CDF5* to dawn, when it induces hypocotyl cell elongation
543 by upregulating growth-related genes like *YUC8*, or *FLA9*. See also Figures S3 and S4.

544 **STAR Methods**

545 **Contact for Reagent and Resource Sharing**

546 Further information and requests for resources and reagents should be directed to and will
547 be fulfilled by the Lead Contact, Elena Monte (elena.monte@cragenomica.es).

548 **Experimental Model**

549 The *Arabidopsis thaliana* (L.) accession Columbia (Col-0), C24, and mutants used here
550 were obtained from the mentioned references or generated in this work (See Key
551 Resources Table).

552 **Method Details**

553 Seedling Growth and Hypocotyl and Cell Measurements

554 *Arabidopsis thaliana* seeds used in this manuscript include the previously described *cdf5*-
555 *1* [19], *toc1-101* [36], *pPRR7::PRR7-GFP* (PRR7-GFP) [27], *pPIF3::YFP:PIF3* (YFP-
556 PIF3) [26], *p35S::PIF4-HA* [25], *pif1-1* [34], *pif3-3* [9], *pif4-2* [37], *pif5-3* [38], *pifq* [37],
557 *prp5-1*, *prp7-3*, and *prp9-1* [39], *pif3-1* [9], *pif4-101* [25], *pil6-1* (*pif5* mutant) [40], and
558 the newly generated *prp7-3pif3-1* (*prp7pif3*), *prp7-3pif4-101* (*prp7pif4*), *prp7-3pil6-1*
559 (*prp7pif5*), *prp7-3prp9-1* (*prp79*), *prp5-1prp9-1* (*prp59*), *prp5-1prp7-3prp9-1* (*prp579*), and
560 *prp7-3cdf5-1* (*prp7cdf5*) in Col-0 ecotype, and *pTOC1::TOC1:YFP* (TMG) [41] in C24
561 ecotype. *CDF5OX* lines were generated by cloning the *CDF5* ORF under the regulation
562 of the 35S promoter in the pH7FWG2 vector. The resulting 35S::*CDF5*-GFP construct
563 was transformed into *cdf5* to generate *CDF5OX* lines, and into *pifq* to generate
564 *pifqCDF5OX* lines.

565 Seeds were sterilized and plated on Murashige and Skoog medium without sucrose.
566 Seedlings were stratified for 4d at 4C in darkness, and seedling growth was done in short
567 days (8h light + 16h dark) or continuous white light ($85\mu\text{mol}\cdot\text{m}^{-2}\cdot\text{s}^{-1}$) for the time
568 indicated in each experiment. Hypocotyl measurements in Figures 2E, 4A and S3B were
569 done using Image J (National Institutes of Health). Saturating FR pulses were $30\mu\text{mol}\cdot\text{m}^{-2}\cdot\text{s}^{-1}$
570 for 15min. Samples at ZT0 and ZT24 were collected in the dark, whereas at ZT8
571 were in the light. For hypocotyl growth rate measurements (Figure 4B), image acquisition
572 was done using the ActiveWebCam software (www.pysoft.com) under infrared light
573 background using modified webcams (Microsoft Life Cam Studio). Twelve seedlings
574 were measured individually every 2 hours throughout the diurnal cycle, the difference in
575 hypocotyl length between the two time points was calculated, and the elongation rate was
576 expressed as mm/h. The mean and SE for the 12 seedlings are represented. Cell size was
577 visualized in seedlings stained with propidium iodine ($10\mu\text{g}/\text{ml}$) (Calbiochem) using a
578 confocal laser microscope Leica SP5 (570 nm-666 nm). Cell length was measured in
579 pictures taken with an optic microscope (AixoPhot DP70) (Figure 4D).

580 ChIP-seq Data Analysis and Visualization

581 Comparison of ChIP-seq data shown in Figure 1A was performed using PIF- [16] and
582 PRR9/7/5-associated peaks from [15], which contained novel PRR9 and re-analyzed
583 ChIP-seq data for PRR5 [22] and PRR7 [42], considering only the PRR binding sites
584 located upstream of the transcriptional start site TSS as in [16]. The same comparison
585 was performed in Figure 1D adding the PIF/SD-induced gene set from [4]. Distance
586 between PIF and PRR peaks was calculated separately for all the different pair-wise
587 combinations associated to a given gene. To jointly visualize the Chip-Seq data for PRR
588 [15] and PIFs [16], and the conserved noncoding sequences (CNS) regions [24] (Figure
589 1E), the Integrated Genome Browser (IGB) [43] was used. Data was obtained from
590 <http://mustang.biol.mcgill.ca> (CNS), GSE71397 (PRRs) and GSE43286 (PIFs).
591 Expression phases shown in Figures 1C and S1C were analyzed using the PHASER tool
592 (<http://phaser.mocklerlab.org>) for SD (Col-0_SD), LD (longday), and LL (LL23_LDHH).
593 The PHASER tool generated over-representation p-values for each phase (Dataset 1).
594 DAVID system [44] was used to identify enriched GO biological terms (Figure S1B).

595 Chromatin Immunoprecipitation (ChIP) Assays

596 Chromatin immunoprecipitation (ChIP) and ChIP-qPCR assays (Figure 2A) were
597 performed as in [5,45]. For PIF3-YFP, all process was performed in the dark under green
598 safelight. Seedlings (3g) were vacuum-infiltrated with 1% formaldehyde and cross-
599 linking was quenched by vacuum infiltration with 0.125 M glycine for 5 min. Tissue was
600 ground, and nuclei-containing cross-linked protein and DNA were purified by sequential
601 extraction on Extraction Buffer 1 (0.4M Sucrose, 10 mM Tris-HCL pH8, 10mM MgCl₂,
602 5mM β-mercaptoethanol, 0.1mM PMSF, 50 μM MG132, proteinase inhibitor cocktail),
603 Buffer 2 (0.25M Sucrose, 10mM Tris-HCL pH8, 10mM MgCl₂, 1% Triton X-100, 5mM
604 β-mercaptoethanol, 0.1mM PMSF, 50 μM MG132, proteinase inhibitor cocktail), and
605 Buffer 3 (1.7M Sucrose, 10 mM Tris-HCL pH8, 0.15% Triton X-100, 2mM MgCl₂, 5mM
606 β-mercaptoethanol, 0.1mM PMSF, 50 μM MG132, proteinase inhibitor cocktail). Nuclei
607 were resuspended in nuclei lysis buffer (50 mM Tris-HCL pH8, 10 mM EDTA, 1 %
608 SDS, 50 μM MG132, proteinase inhibitor cocktail), sonicated for 10X 30sec, and diluted
609 10X in Dilution Buffer (0.01% SDS, 1% Triton X-100, 1.2 mM EDTA, 16.7 mM Tris-
610 HCL pH8, 167 mM NaCl). Overnight incubation was performed with the corresponding
611 antibody (or with no antibody as control) at 4C overnight, and immunoprecipitation was
612 performed using dynabeads. Washes were done sequentially in Low Salt Buffer (0.1%
613 SDS, 1% Triton X-100, 2 mM EDTA, 20 mM Tris-HCL pH8, 150 mM NaCl), High Salt
614 Buffer (0.1% SDS, 1% Triton X-100, 2 mM EDTA, 20 mM Tris-HCL pH8, 500 mM
615 NaCl), LiCl Buffer (0.25M LiCl, 1% NP40, 1% deoxycholic acid sodium, 1 mM EDTA,
616 10 mM Tris-HCL pH8), and TE X1. Immunocomplexes were eluted in Elution Buffer
617 (1%SDS, 0.1M NaHCO₃), de-crosslinked overnight at 65C in 10 mM NaCl, and then
618 treated with proteinase K. DNA was purified using Qiagen columns, eluted in 100 uL of
619 Qiagen elution buffer, and 2 uL were used for qPCR (ChIP-qPCR) using *CDF5*
620 promoter-specific primers (Table S1) spanning the region containing the predicted
621 binding sites for the PIFs [16]. Three biological replicates were performed for all the
622 “Antibody” samples (two for WT TMG at ZT8), and one for the “No Antibody”.
623 Calculations of percent input were done following the protocol available at
624 www.thermofisher.com.

625 Yeast Two-Hybrid Assays

626 For yeast two-hybrid assays shown in Figure S1A, we used PIF3 (pGAD424) and PIF4
627 (pGADT7) described previously [7,46]. PRR fragments were PCR-amplified from PRR
628 templates [47] with primers containing restriction sites (XmaI/BamHI for PRR5 and
629 PRR9, EcoRI/XmaI for PRR7) (Table S1), cloned into pTOPO vector (NZYTech),
630 sequenced and cloned into pGBKT7 (Clontech). To assess interactions, constructs were
631 co-transformed into yeast AH109 cells (Clontech). Yeast transformants were selected on
632 synthetic dropout medium (SD) deficient in leucine and tryptophan (-LT), and interaction
633 was assayed quantitatively by a β -Galactosidase assay performed using ortho-
634 nitrophenyl- β -D-galacpyranoside as a substrate following manufacturer's instructions.

635 Bimolecular Fluorescence Complementation (BiFC) Assays

636 For bimolecular fluorescence complementation (BiFC) shown in Figure 1B, the coding
637 regions of PIF3 and TOC1 [5] were cloned into pGWcY and pGWnY vectors [48],
638 respectively. PRR5-, PRR7- and PRR9-nYFP are from [47]. Preparation of samples and
639 bombardment of onion cells were done as in [5]. Briefly, the inner layers of spring onions
640 were cut in 2 x 2 cm squares and used for particle bombardment. Each sample was
641 transfected with 1 μ g of each plasmid coupled to tungsten particles using a Biolistic
642 Particle Delivery System PDS-1000 (Bio-Rad). After bombardment, onions were
643 exposed to a saturating 15 min FR pulse and incubated overnight in dark conditions. The
644 upper epidermal layer was removed, placed in a microscope slide and visualized using a
645 confocal laser scanning microscope Olympus FV1000 (Objective Lens UPLSAPO 20X,
646 Laser Wavelength: 514 nm, Emission window: 525-600 nm).

647 Protein Extraction and Immunoblot

648 Total protein extracts to detect endogenous PIF3 were prepared from 3 day-old SD-
649 grown seedlings harvested at ZT24 in the dark (Figure 2D). Total protein extracts to
650 detect endogenous PIF3 were prepared from 3 day-old SD-grown seedlings harvested at
651 ZT24 in the dark (Figure 2D). Extraction buffer and protein quantification were done
652 essentially as described [49]: Samples were collected and frozen in liquid nitrogen, and
653 manually ground under frozen conditions before resuspension in boiling extraction buffer
654 (100 mM MOPS (pH 7.6), 2% SDS, 10% glycerol, 4mM EDTA, 50mM Sodium
655 metabisulfite ($\text{Na}_2\text{S}_2\text{O}_5$), 2 g l^{-1} aprotinin, 3 g l^{-1} leupeptin, 1 g l^{-1} pepstatin and 2 mM

656 PMSF). Total protein was quantified using a Protein DC kit (Bio-Rad), and β -
657 mercaptoethanol was added just before loading. Aliquots of 100 ug for each sample were
658 treated for 5min at 95C and subjected to 12.5% SDS- PAGE gels. Proteins were then
659 transferred to Immobilon-P membrane (Millipore), and immunodetection of endogenous
660 PIF3 was performed using a anti-PIF3 antibody [26] (1:10,000 dilution) incubated with
661 Hikari solution (Nacalai Tesque). Peroxidase-linked anti rabbit secondary antibody
662 (1:5,000 dilution) and a SuperSignal West Femto chemiluminescence kit (Pierce) were
663 used for detection of luminescence using LAS-4000 Image imaging system (Fujifilm).
664 The membrane was stained with Coomassie blue as a loading control.

665 Gene Expression Analysis

666 Quantitative RT-PCR, RNA extraction, cDNA synthesis and qRT-PCR were done as
667 described [49]. Briefly, 1 mg of total RNA extracted using the RNeasy Plant Mini Kit
668 (Qiagen) were treated with DNase I (Ambion) according to the manufacturer's
669 instructions. First-strand cDNA synthesis was performed using the SuperScript III
670 reverse transcriptase (Invitrogen) and oligo dT as a primer (dT30). cDNA was then
671 treated with RNase Out (Invitrogen) before 1:20 dilution with water, and 2 ul was used
672 for real-time PCR (Light Cycler 480; Roche) using SYBR Premix Ex Taq (Takara) and
673 primers at a 300 nM concentration. Gene expression in time-course analyses (Figures 2C,
674 3A, 3B, 3D, 3E, S2C and S2D) was measured in two independent biological replicates,
675 with three technical replicates for each biological sample, and the mean of the biological
676 replicates \pm SE is shown. For specific time points in Figures 2B, 4C, S2A, S2B, and S3C,
677 gene expression was measured in three independent biological replicates, and in Figure
678 3C, corresponds to two biological replicates, with three technical replicates for each
679 biological sample. *PP2A* (*ATIG13320*) was used for normalization.

680 **Quantification and Statistical Analysis**

681 Differences between means were statistically analyzed by one-way analysis of variance
682 using Tukey-b post hoc multiple comparison test (IBM SPSS Statistics Software) or
683 homoscedastic Student's t-test (Excel Microsoft), as indicated in the figure legends.
684 Statistically significant differences were defined as those with a P value < 0.05.
685 Significance level is indicated as * P < 0.05, ** P < 0.01 and *** P < 0.001.

686 **Supplemental Tables**

687 Dataset 1: Comparison of genome-wide loci associated to PIFs and PRR9, 7 and 5.
688 Related to Figure 1.

689 Table S1: List of Oligonucleotides. Related to STAR Methods.

690

TABLE FOR AUTHOR TO COMPLETE

Please upload the completed table as a separate document. **Please do not add subheadings to the Key Resources Table.** If you wish to make an entry that does not fall into one of the subheadings below, please contact your handling editor. (NOTE: For authors publishing in *Current Biology*, please note that references within the KRT should be in numbered style, rather than Harvard.)

KEY RESOURCES TABLE

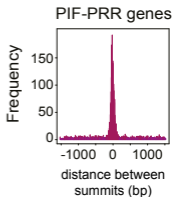
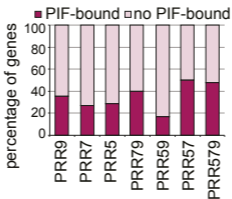
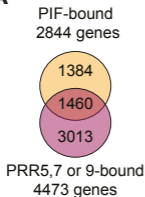
REAGENT or RESOURCE	SOURCE	IDENTIFIER
Antibodies		
Anti-GFP	Invitrogen	Cat# A11122
Peroxidase-linked anti rabbit secondary antibody	Sigma	Cat# NA934
Anti-PIF3	[26]	N/A
Anti-HA	Abcam	Cat# 9110
Bacterial and Virus Strains		
AH109	Clontech	N/A
<i>E. coli</i> DH5 α	N/A	N/A
<i>A. tumefaciens</i> GV3031	N/A	N/A
Chemicals, Peptides, and Recombinant Proteins		
Formaldehyde	ThermoFisher Scientific	Cat# 28908
Glycine	GE Healthcare Life Sciences	Cat# 17-1323-01
EDTA	Thermo Scientific	Cat# 17892
Tris-HCL	Sigma	Cat# C4706-2G
Proteinase K	ThermoFisher Scientific	Cat# EO0491
Sucrose	Applichem	Cat# A1125.1000
MgCl ₂	Calbiochem	Cat# 442611
PMSF	Applichem	Cat# A0999,0025
MG132	Merck	Cat# 474790
Proteinase Inhibitor Cocktail	Roche	Cat# 4693116001
Triton X-100	Applichem	Cat# A1388.10000
NaCl	Scharlau	Cat# SO02271000
LiCl	Merck	Cat# 1,056,790,250
NP40	Sigma	Cat# 74385
Deoxycholic acid sodium	Sigma	Cat# D6750
NaHCO ₃	Merck	Cat# 6329
Dropout medium (-AHLT)	Clontech	Cat# 630428
Yeast Nitrogen Base w/o aa & ammonium sulfate	Conda	Cat# 1553.00
Ammonium Sulfate	Sigma	Cat# A4418
D-Glucose	Applichem	Cat# 3O000431
European bacteriological Agar	Conda	Cat# 1800.00
His	Sigma	Cat# H8125
Trp	Sigma	Cat# T0254
Leu	Sigma	Cat# L8912
Ade	Sigma	Cat# A9126

Propidium iodine	Calbiochem	Cat# 537059-
Ortho-nitrophenyl- β -D-galacpyranoside	ThermoFisher Scientific	Cat# 34055
DNase I	Ambion	Cat# AM2224
RNase Out	Invitrogen	Cat# 10777019
SYBR Premix Ex Taq	Roche	Cat# 04707516001
MOPS (pH 7.6)	Sigma	Cat# M1254
SDS	Amresco	Cat# 0227
Glycerol	Applichem	Cat# A2926
EDTA	Thermo Scientific	Cat# 17892
Aprotinin	Applichem	Cat# A2132
Leupeptin	Applichem	Cat# A2183
Pepsatin	Applichem	Cat# A2205
PMSF	Applichem	Cat# A0999
β -mercaptoethanol	Fluka	Cat# 03700
GFP Agarose Beads	MBL	Cat# D153-8
rProtein A-Sepharose	Bionova	Cat# 1-888-752-2568
Hikari solution	Nacalai Tesque	Cat# 02270-81
Sodium metabisulfite	Sigma	Cat# 255556
Xmal	Roche	Cat# ER0171
BamHI	Roche	Cat# 10 220 612 001
EcoRI	Roche	Cat# 10 703 737 001
T4 DNA Ligase	NZYtech	Cat# MB00703
BP Clonase II	Gateway	Cat# 11789-020
LR Clonase II	Gateway	Cat# 11791-020
Critical Commercial Assays		
RNeasy Plant Mini	Qiagen	Cat# 74904
SuperScript III reverse transcriptase	Invitrogen	Cat# 18080044
Protein DC	Bio-Rad	Cat# 5000121
SuperSignal West Femto chemiluminescence	Thermo Scientific	Cat# 34095
QIAquick gel extraction kit	Qiagen	Cat# QIA28704
Dynabeads	Invitrogen	Cat# 10004D
Immobilon-P membrane	Millipore	Cat# IPVH00010
Experimental Models: Organisms/Strains		
Col-0	N/A	N/A
C24	N/A	N/A
<i>cdf5-1</i>	[19]	N/A
<i>toc1-101</i>	[36]	N/A
<i>pPRR7::PRR7-GFP</i> (PRR7-GFP)	[27]	N/A
<i>pPIF3::YFP:PIF3</i> (YFP-PIF3)	[26]	N/A
<i>p35S::PIF4-HA</i> (PIF4-HA)	[25]	N/A
<i>pTOC1::TOC1:YFP</i> (TMG)	[41]	N/A
<i>pif1-1</i>	[34]	N/A
<i>pif3-3</i>	[9]	N/A
<i>pif4-2</i>	[37]	N/A

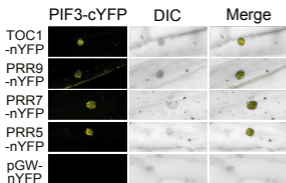
<i>pif5-3</i>	[38]	N/A
<i>pifq</i>	[37]	N/A
<i>prr5-1</i>	[39]	N/A
<i>prr7-3</i>	[39]	N/A
<i>prr9-1</i>	[39]	N/A
<i>pif3-1</i>	[9]	N/A
<i>pif4-101</i>	[25]	N/A
<i>pil6-1 (pif5)</i>	[40]	N/A
<i>prr7-3pif3-1 (prr7pif3)</i>	This paper	N/A
<i>prr7-3pif4-101 (prr7pif4)</i>	This paper	N/A
<i>prr7-3pil6-1 (prr7pif5)</i>	This paper	N/A
<i>prr7-3prr9-1 (prr79)</i>	This paper	N/A
<i>prr5-1prr9-1 (prr59)</i>	This paper	N/A
<i>prr5-1prr7-3prr9-1 (prr579)</i>	This paper	N/A
<i>prr7-3cdf5-1 (prr7cdf5)</i>	This paper	N/A
<i>35S::CDF5-GFP (CDF5OX)</i>	This paper	N/A
<i>pifqCDF5OX</i>	This paper	N/A
<i>pifqcdf5</i>	This paper	N/A
Oligonucleotides		
See Table S2	N/A	N/A
Recombinant DNA		
pH7FWG2	Gateway	N/A
PIF3 in pGAD424	[46]	N/A
PIF4 in pGADT7	[7]	N/A
NZY-A PCR cloning kit	NZYTech	Cat# MB05302
pGBKT7	Clontech	Cat# PT3248-5
pGWcY	[48]	N/A
pGWnY	[48]	N/A
Software and Algorithms		
ActiveWebCam software (www.pysoft.com)	N/A	N/A
Integrated Genome Browser (IGB)	[43]	N/A
PHASER (http://phaser.mocklerlab.org)	N/A	N/A
DAVID system	[44]	N/A
IBM SPSS Statistics Software	N/A	N/A
Excel	N/A	N/A

Figure 1

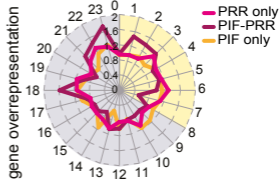
A



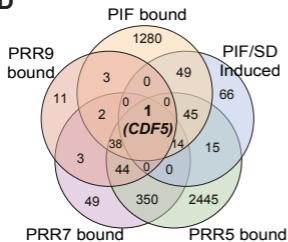
B



C



D



E

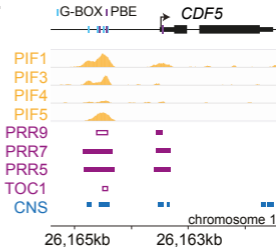
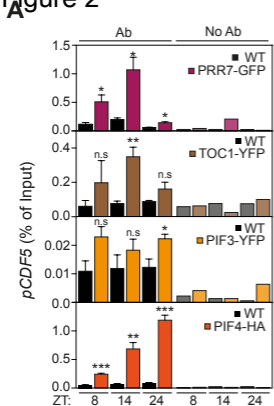
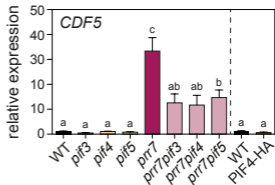


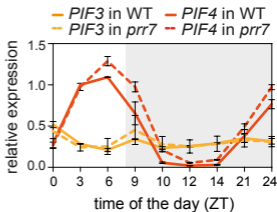
Figure 2



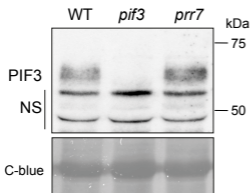
B



C



D



E

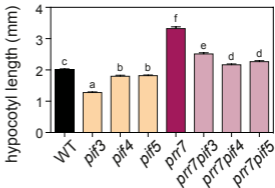


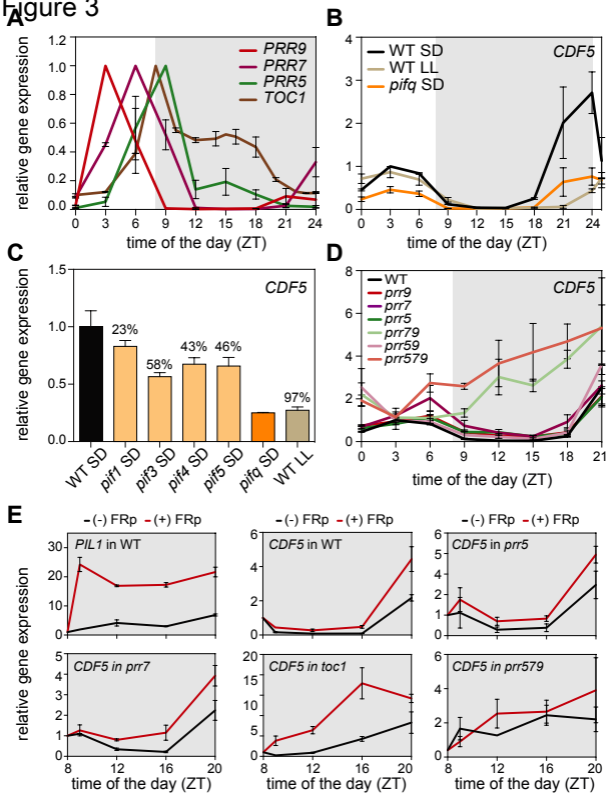
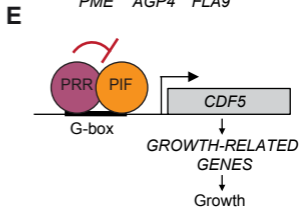
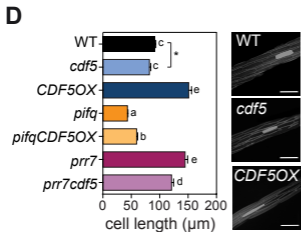
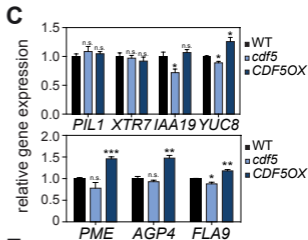
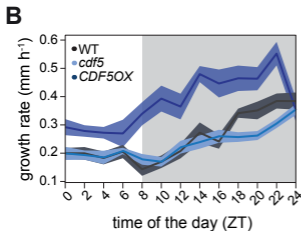
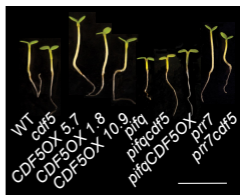
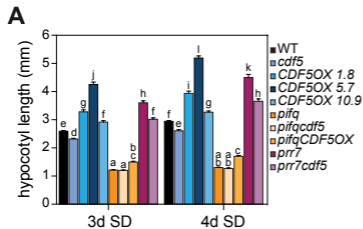
Figure 3

Figure 4



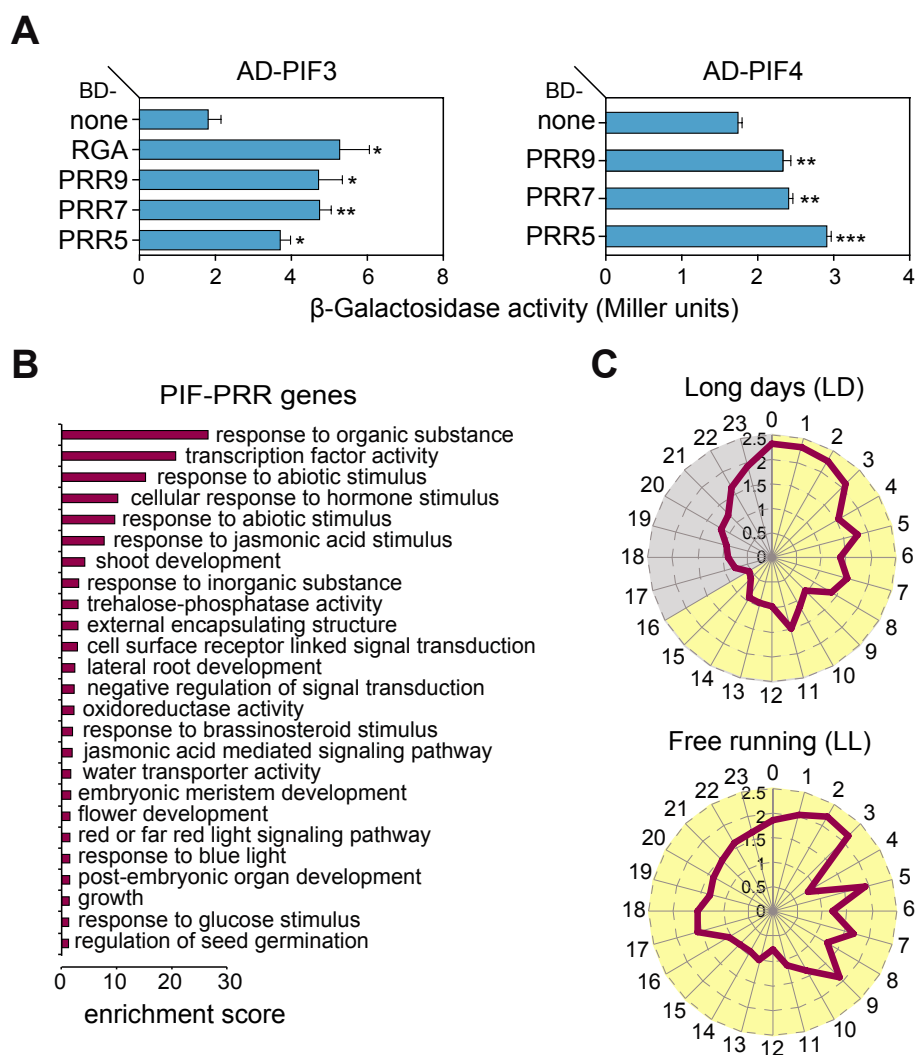


Figure S1. Related to Figure 1. Yeast-two-hybrid assays showing the interaction between PIF3, PIF4, and PRR9/7/5, and gene ontology (GO) and phaser analysis in LD and LL of PIF-PRR genes. (A) β -galactosidase activities from yeast two-hybrid assays showing interactions between PIF3 (left), PIF4 (right) and PRR5, PRR7, and PRR9. Error bars indicate SE ($n = 3$). Significance level is relative to the BD alone control (* $P < 0.05$; ** $P < 0.01$ and *** $P < 0.001$). DELLA protein RGA is included as positive control for PIF3 interactions [S1]. **(B)** Cluster analysis of the most enriched GO annotations for PIF-PRR genes. **(C)** Comparison of expression phases in long days (top) and free running (bottom) conditions of the 1,460 “PIF-PRR” gene set defined in Figure 1A and provided in Dataset 1. Phases as defined by PHASER (phaser.mocklerlab.org) are indicated on the circumference, and fold-change phase enrichment of genes (count/expected) is shown on the radius. Day is shown in yellow; night is shown in grey.

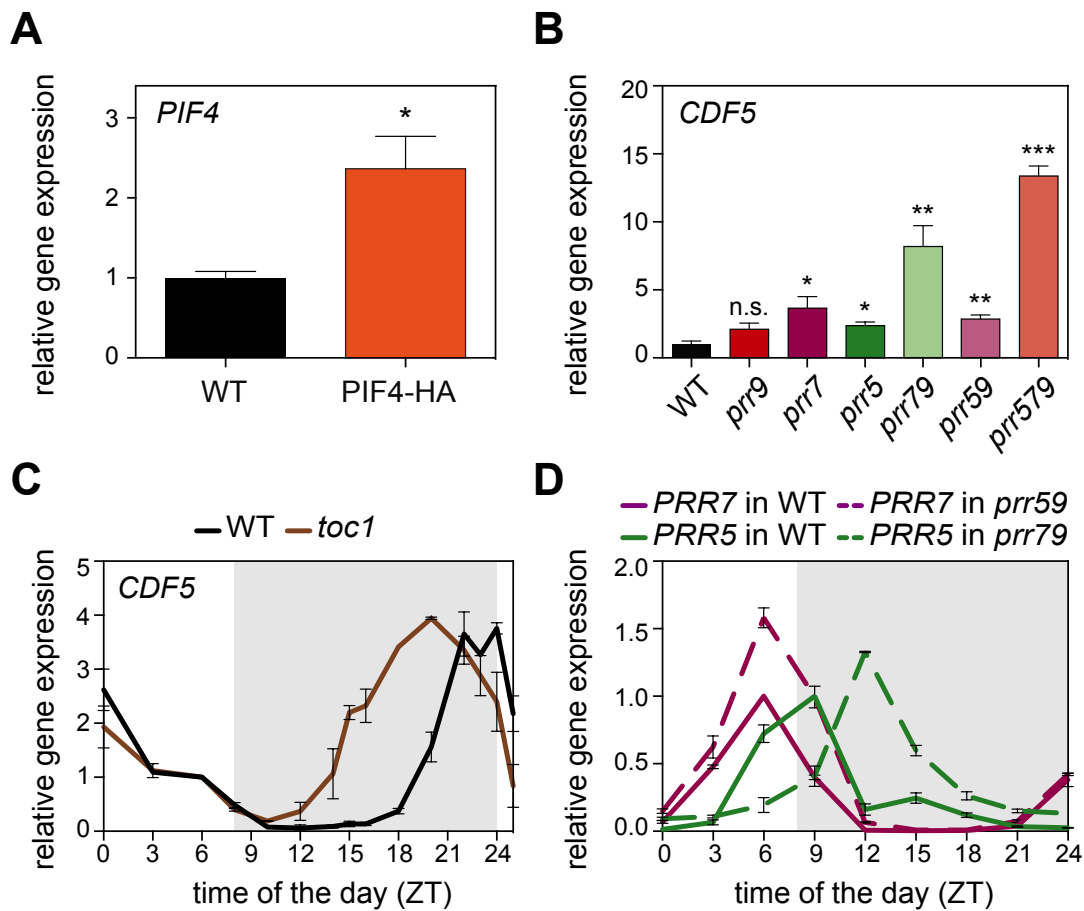


Figure S2. Related to Figures 2 and 3. *PIF4*, *CDF5*, *PRR5* and *PRR7* expression analyses in *PIF4*-HA overexpressing plants, and in *toc1*, *prr5*, *prr7*, and *prr9* single and higher order mutant combinations. *PIF4* expression in WT and *35S::PIF4-HA* (*PIF4*-HA) seedlings at ZT8 (A) and *CDF5* expression in WT and *prr* mutants at ZT9 (B) during the third day of growth in SD. Data are from three independent biological replicates relative to WT set at one. Error bars indicate SE. Statistically significant differences between mean values by Student's *t*-test relative to WT are shown (* $P < 0.05$; ** $P < 0.01$ and *** $P < 0.001$). n.s., not significant. (C) *CDF5* expression in WT and *toc1*. (D) *PRR5* and *PRR7* expression in WT and *prr79* and *prr59*, respectively. (C, D) Seedlings were grown for 2 days in SD and harvested during the third day at the indicated times. Data plotted are mean \pm SE relative to ZT6 for each genotype (C) or relative to its maximum expression value set at one for each gene (D), $n = 2$ independent biological experiments, each assayed in triplicate. (A-D) All samples were analyzed by qRT-PCR and normalized to *PP2A*.

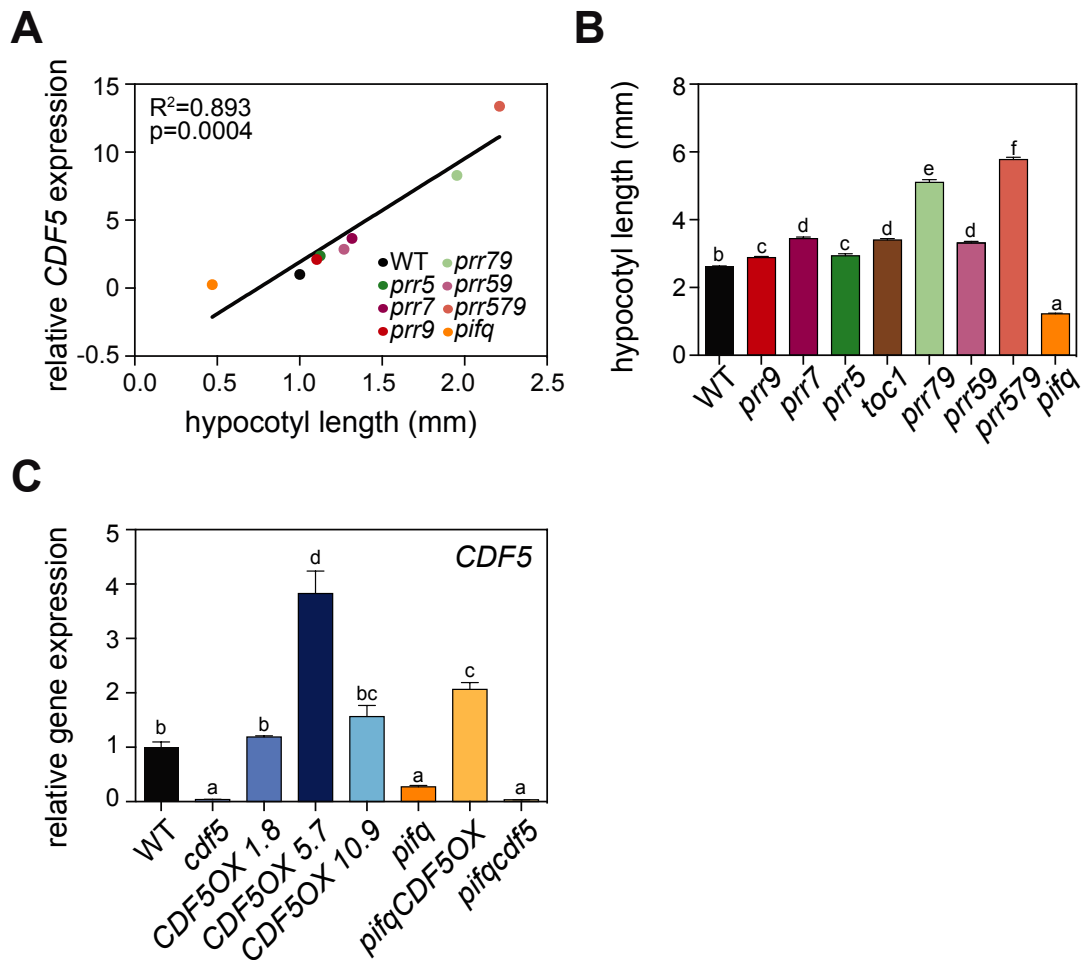


Figure S3. Related to Figures 3 and 4. *CDF5* expression in correlation with hypocotyl length and in generated *CDF5* mutant lines. (A) *CDF5* expression levels correlate with hypocotyl length. Correlation of hypocotyl length in (B) with *CDF5* expression values of WT, *prr* and *toc1* in 2-day-old SD-grown seedlings harvested at ZT9 during the third day under SD. *pifq* expression values are from Figure S2A. **(B)** Quantification of hypocotyl elongation in 3-day-old SD-grown WT, *prr*, *toc1*, and *pifq* seedlings. Data are means \pm SE of at least 50 seedlings. **(C)** Characterization of *CDF5* expression levels in *CDF5OX* mutant lines. *CDF5* expression in 3-d-old SD-grown WT, *cdf5*, *CDF5OX*, *pifq*, *pifqCDF5OX*, and *pifqcdf5* seedlings at ZT24. In (A) and (C), expression was analyzed by qRT-PCR, and values were normalized to *PP2A* and are shown relative to WT levels set at one. Data are from three independent biological replicates. In (C) error bars indicate SE. Different letters shown in (B) and (C) denote statistically significant differences among means by Tukey-b test ($P<0.05$).

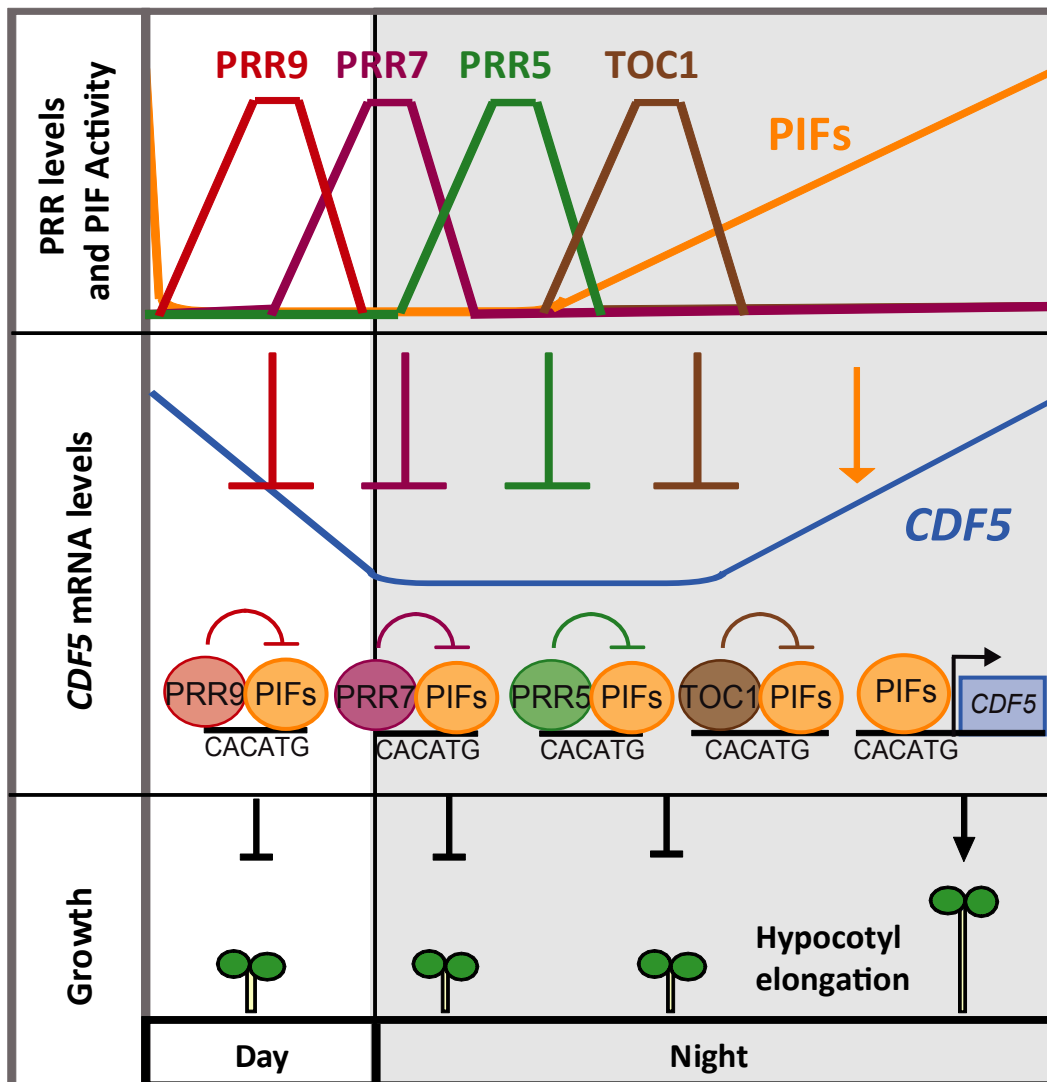


Figure S4. Related to Figure 4. Model of the proposed role of PRRs as repressors of PIF activity in gating CDF5-mediated elongation. Sequential PRR9/7/5 and PRR1/TOC1 accumulation from morning to midnight (top) represses PIF-induction of *CDF5*, a transcription factor necessary for growth-promotion (middle). PIFs are present during the day and progressively accumulate during the night concurrently to a decline in PRRs and TOC1 abundance (top). At predawn, PRRs and TOC1 are no longer present, repression on the PIFs is lifted (top), and PIFs induce *CDF5* expression (middle) to promote hypocotyl elongation (bottom). Based on current data, PRRs and PIFs could bind to the same or different nearby G-boxes, PIFs might bridge the binding of PRRs to DNA, or PRRs could compete with PIFs for binding to G-boxes.

Supplemental References

- S1. Feng, S., Martinez, C., Gusmaroli, G., Wang, Y., Zhou, J., Wang, F., Chen, L., Yu, L., Iglesias-Pedraz, J.M., Kircher, S., *et al.* (2008). Coordinated regulation of Arabidopsis thaliana development by light and gibberellins. *Nature* *451*, 475–479.
- S2. Pfeiffer, A., Shi, H., Tepperman, J.M., Zhang, Y., and Quail, P.H. (2014). Combinatorial Complexity in a Transcriptionally Centered Signaling Hub in Arabidopsis. *Mol. Plant* *7*, 1598–1618.
- S3. Liu, T.L., Newton, L., Liu, M.-J., Shiu, S.-H., and Farré, E.M. (2016). A G-Box-Like Motif Is Necessary for Transcriptional Regulation by Circadian Pseudo-Response Regulators in Arabidopsis. *Plant Physiol.* *170*, 528–539.
- S4. Martín, G., Soy, J., and Monte, E. (2016). Genomic Analysis Reveals Contrasting PIFq Contribution to Diurnal Rhythmic Gene Expression in PIF-Induced and - Repressed Genes. *Front. Plant Sci.* *7*, 962.
- S5. Fornara, F., Panigrahi, K.C.S., Gissot, L., Sauerbrunn, N., Rühl, M., Jarillo, J.A., and Coupland, G. (2009). Arabidopsis DOF Transcription Factors Act Redundantly to Reduce CONSTANS Expression and Are Essential for a Photoperiodic Flowering Response. *Dev. Cell* *17*, 75–86.
- S6. Mockler, T.C., Yu, X., Shalitin, D., Parikh, D., Michael, T.P., Liou, J., Huang, J., Smith, Z., Alonso, J.M., Ecker, J.R., *et al.* (2004). Regulation of flowering time in Arabidopsis by K homology domain proteins. *Proc. Natl. Acad. Sci. U. S. A.* *101*, 12759–12764.
- S7. Soy, J., Leivar, P., González-Schain, N., Martín, G., Diaz, C., Sentandreu, M., Al-Sady, B., Quail, P.H., and Monte, E. (2016). Molecular convergence of clock and photosensory pathways through PIF3–TOC1 interaction and co-occupancy of target promoters. *Proc. Natl. Acad. Sci. U. S. A.* *113*, 4870–4875.
- S8. Soy, J., Leivar, P., González-Schain, N., Sentandreu, M., Prat, S., Quail, P.H., and Monte, E. (2012). Phytochrome-imposed oscillations in PIF3 protein abundance regulate hypocotyl growth under diurnal light/dark conditions in Arabidopsis. *Plant J.* *71*, 390–401.
- S9. http://www.tdx.cat/bitstream/handle/10803/130896/MGR_TESIS.pdf.
- S10. Rawat, R., Schwartz, J., Jones, M.A., Sairanen, I., Cheng, Y., Andersson, C.R., Zhao, Y., Ljung, K., and Harmer, S.L. (2009). REVEILLE1, a Myb-like transcription factor, integrates the circadian clock and auxin pathways. *Proc. Natl. Acad. Sci. U. S. A.* *106*, 16883–16888.
- S11. Shin, J., Park, E., and Choi, G. (2007). PIF3 regulates anthocyanin biosynthesis in an HY5-dependent manner with both factors directly binding anthocyanin biosynthetic gene promoters in Arabidopsis. *Plant J.* *49*, 981–994.

1 **Circadian waves of transcriptional repression shape PIF-regulated photoperiod-**
2 **responsive growth in Arabidopsis**

3 Guiomar Martín¹, Arnau Rovira¹, Nil Veciana¹, Judit Soy¹, Gabriela Toledo-Ortiz^{3,4},
4 Charlotte M. M. Gommers¹, Marc Boix¹, Rossana Henriques¹, Eugenio G. Minguet²,
5 David Alabadi², Karen Halliday⁴, Pablo Leivar^{1,5}, and Elena Monte^{1,6,7,*}

6 ¹Center for Research in Agricultural Genomics (CRAG), CSIC-IRTA-UAB-UB, Campus
7 UAB, Edifici CRAG, Bellaterra, 08193 Barcelona, Spain.

8 ²Instituto de Biología Molecular y Celular de Plantas (IBMCP), CSIC-UPV, Ingeniero
9 Fausto Elio s/n, 46022 Valencia, Spain

10 ³Lancaster Environment Center, Lancaster University. Lancaster, LA1 4YQ, UK.

11 ⁴The University of Edinburgh. CH Waddington Building, Max Born Crescent,
12 Edinburgh, EH9 3BF, UK.

13 ⁵Bioengineering Department, IQS School of Engineering. Via Augusta 390, 08017
14 Barcelona, Spain.

15 ⁶Consejo Superior de Investigaciones Científicas (CSIC), 08028 Barcelona, Spain.

16 ⁷Lead contact

17 *Corresponding author: elena.monte@cragenomica.es

18

19 **Summary**

20 Plants coordinate their growth and development with the environment through integration
21 of circadian clock and photosensory pathways. In *Arabidopsis thaliana*, rhythmic
22 hypocotyl elongation in short days (SD) is enhanced at dawn by the bHLH transcription
23 factors PHYTOCHROME-INTERACTING FACTORS (PIFs) directly inducing
24 expression of growth-related genes [1–6]. PIFs accumulate progressively during the night
25 and are targeted for degradation by active phytochromes in the light, when growth is
26 reduced. Although PIF proteins are also detected during the day hours [7–10], their
27 growth-promoting activity is inhibited through unknown mechanisms. Recently, the core
28 clock components and transcriptional repressors PSEUDO-RESPONSE REGULATORS
29 PRR9/7/5 [11,12], negative regulators of hypocotyl elongation [13,14], were described to
30 associate to G-boxes [15], the DNA motifs recognized by the PIFs [16,17], suggesting
31 that PRR and PIF function might converge antagonistically to regulate growth. Here we
32 report that PRR9/7/5 and PIFs physically interact and bind to the same promoter region
33 of pre-dawn-phased, growth-related genes, and we identify the transcription factor CDF5
34 [18,19] as target of this interplay. In SD, *CDF5* expression is sequentially repressed from
35 morning to dusk by PRRs and induced pre-dawn by PIFs. Consequently, *CDF5*
36 accumulates specifically at dawn, when it induces cell elongation. Our findings provide a
37 framework for recent TIMING OF CAB EXPRESSION 1 (TOC1/PRR1) data [5,20] and
38 reveal that the long described circadian morning-to-midnight waves of the PRR
39 transcriptional repressors (PRR9, PRR7, PRR5 and TOC1) [21] jointly gate PIF activity
40 to dawn to prevent overgrowth through sequential regulation of common PIF-PRR target
41 genes such as *CDF5*.

42

43 **Results and Discussion**

44 Genome-wide analysis of ChIP-sequencing (ChIP-seq) data for the PIF quartet (PIFq)
45 (PIF1, 3, 4, 5)-associated [16] and PRR5-, PRR7-, and/or PRR9-associated [15] loci
46 revealed an overlap of 1,460 genes between PIF-bound genes (57.5 % of all PIF-bound
47 genes) and at least one of the three PRRs examined (“PIF-PRR genes”) (Figure 1A left;
48 Dataset 1). The overlap between PIF-bound and PRR5-, PRR7-, or PRR9-bound, when
49 examined individually or in combination, is shown in Figure 1A middle (Dataset 1).
50 Distance between PRR and PIF binding sites indicate that PRRs and PIFs associate to the
51 same genomic regions (Figure 1A right), in accordance with results showing enrichment
52 of G-box-containing motifs in PRR-bound regions [15,22]. We detected interaction of
53 PIF3 and PIF4 with PRR5 (PIF4 in accordance to [20]), PRR7 and PRR9 by yeast two-
54 hybrid assays (Figure S1A). We further confirmed PIF3-PRR interaction *in planta* by
55 BiFc assays (Figure 1B). These data suggest that, similarly to recent findings for TOC1
56 and PIF3 and PIF4 [5,20], PIFs and PRRs may bind together at G-boxes to co-regulate
57 the expression of shared PIF-PRR target genes. Based on the described activity of PRRs
58 as transcriptional repressors [11,12,20], PIF-PRR interaction also agrees with the
59 possibility that PRR5/7/9 might target PIFs to repress their ability to activate shared PIF-
60 PRR target genes as shown recently for TOC1 and PIFs [5,20].

61 Functional classification indicated that “PIF-PRR” genes are enriched in growth-related
62 categories (Figure S1B) and are overrepresented at the elongation phases 18-23
63 specifically under SD (Figure 1C, Figure S1C) (Dataset 1), suggesting that PIFs and
64 PRRs jointly target genes involved in the induction of growth under SD conditions. We
65 compared PRR- and PIF-bound genes with the recently defined PIF- and SD-induced
66 (PIF/SD-induced) gene set of PIFq-regulated genes under SD containing dawn-phased
67 and growth-related genes [4]. Strikingly, one gene (*CDF5*) was PIF/SD-induced and
68 bound by all PRRs and PIFs (Figure 1D, Dataset 1). Previous ChIP experiments showed
69 binding of PRR5/7/9 and possibly TOC1 to this G-box/PBE containing region [15,22,23]
70 (Figure 1E, see legend for details). This region coincides with conserved noncoding
71 sequences (CNS) among crucifer regulatory regions (Figure 1E) [24], suggesting that the
72 binding sites on the *CDF5* promoter have been subjected to selective constraint,
73 consistent with functionality relevance.

74 We verified binding of PRR7, TOC1, PIF3 and PIF4 to the *CDF5* promoter (*pCDF5*)
75 region encompassing the G-boxes at different times under SD conditions by time-course
76 analysis using ChIP-qPCR. Statistically significant and robust PRR7 binding to *pCDF5*
77 was observed at ZT8 and ZT14, and was substantially decreased at ZT24, whereas
78 maximum of TOC1 binding was at ZT14 (Figure 2A). For PIF3 and PIF4, tagged lines
79 driven by the endogenous PIF3 promoter and 35S were used, respectively [25,26] (Figure
80 S2A). Statistically significant binding of PIF3 to *pCDF5* was detected at ZT24, whereas
81 significant PIF4 binding was detected in all three time points and incremented along the
82 night (Figure 2A). These binding dynamics are consistent with the pattern of
83 accumulation of each protein in SD [5,8,27]. Together, these data are consistent with
84 binding of the PIFs, PRRs and TOC1 proteins in SD to the same region of the *CDF5*
85 promoter located approximately 1000 bp upstream of the TSS, and with binding dictated
86 by their protein abundance.

87 To examine how PIF and PRR7 interaction (Figures 1B and S1A) and binding to the
88 *CDF5* promoter (Figure 2A) affect *CDF5* expression, we first tested *CDF5* expression in
89 *pif* and *prr7* mutants under SD at ZT9 when PRR7 levels are maximum and PIFs start to
90 accumulate [7,8,10,27,28]. *CDF5* levels were upregulated in *prr7* (Figure 2B), an effect
91 strongly suppressed by the *pif* mutations in the *prr7pif* double mutants (Figure 2B),
92 suggesting that PIFs and PRR7 regulate *CDF5* expression antagonistically as
93 transcriptional activator and repressor, respectively. Interestingly, because PIF3 transcript
94 and protein levels are not affected in *prr7* (Figures 2C and 2D), together these data
95 suggest that, as described for TOC1 [5], PRR7 acts directly as transcriptional repressor of
96 PIF3 activity in the regulation of *CDF5*. In agreement, the *prr7* long hypocotyl
97 phenotype was also partially suppressed with genetic removal of PIF3 (Figure 2E).
98 However, because the detected binding of PIF3 to the *CDF5* promoter at ZT9 or ZT14
99 was not statistically significant (Figure 2A), we cannot discard that the effect of PRRs on
100 PIF3 might involve inhibition of PIF3 binding to *CDF5* promoter. Suppression of
101 hypocotyl phenotype was also observed for *prr7pif4* and *prr7pif5* compared to *prr7*
102 (Figures 2B and 2E), which suggests that PRR7 directly represses PIF4 transcriptional
103 activity, as previously shown for TOC1 and PIF4 [20], and might also repress PIF5. This
104 scenario might be potentially more complex given that *PIF4/5* transcription is regulated

105 by the clock under SD [2] and at least *PIF4* transcript levels are slightly higher in *prp7*
106 (Figure 2C), in accordance with recent data showing *PIF4* de-repression in *prp* multiple
107 mutants [29]. However, the observation that *CDF5* expression in overexpressing PIF4-
108 HA lines at ZT8 was similar to *pif4* (Figure 2B), a time point where both PRR7 and PIF4
109 are co-bound to the *pCDF5* (Figure 2A), provides strong support that PRR7 directly
110 suppresses PIF4 transcriptional activation activity towards *CDF5*.

111 We next examined the antagonistic PIF-PRR interaction in the direct regulation of *CDF5*
112 across the diurnal cycle. Under SD, phytochrome imposes oscillation of PIF3 and
113 probably PIF1 proteins to progressively accumulate during the night, and to degrade
114 rapidly in the morning maintaining residual levels during the day [8,9]. For PIF4 and
115 possibly PIF5, clock and light regulation result in PIF accumulation also during daytime
116 (Figure 2C) [7,10]. In contrast, PRR accumulation is sequential (PRR9/7/5/TOC1) from
117 morning to midnight (Figure 3A) [21,27]. We therefore expected *CDF5* to oscillate with
118 a peak in the early morning and at the end of the night (where presence of the PIFs is
119 maximum) and a trough from morning to midnight (when PRRs accumulate). Indeed,
120 *CDF5* in the WT was detected during the first part of the day (ZT0-ZT3), then declined
121 to almost undetectable levels through ZT15, and accumulated after ZT15 to peak at dawn
122 (Figure 3B). Expression in *pifq* SD and in WT LL at dawn (a condition where PIFs do not
123 accumulate) [28] was lower than WT SD (Figure 3B), supporting the notion that
124 transcript induction leading to the oscillatory pattern of *CDF5* expression in SD depends
125 on the presence of the PIFs (Figure 3B). Analysis of *CDF5* levels in single *pif* and
126 multiple *pifq* (defective in PIF1/3/4/5) mutants at ZT24 showed that the PIF quartet
127 (PIFq) collectively induces *CDF5* expression at dawn, with PIF1 having a lesser
128 contribution (Figure 3C). *CDF5* transcript levels dropped in the WT after 1h of morning
129 light (Figure 3B), concurrent with phy-induced PIF degradation. In contrast, at ZT9,
130 when *CDF5* expression in the WT is almost non-detectable, *CDF5* expression was
131 significantly higher in *prp5*, *prp7*, *prp79*, *prp59*, and *prp579*, with a major contribution for
132 PRR7 (Figure S2B). Compared to WT, *CDF5* expression was higher in *prp7* from ZT3
133 through midnight (Figure 3D), whereas in *prp59* and *prp79* mutants *CDF5* expression
134 was only slightly higher at dawn in *prp59* and higher from dusk to dawn in *prp79* (Figure
135 3D). In *toc1*, de-repression of *CDF5* was early compared to WT (Figure S2C), similar to

136 other PIF-TOC1 co-targets [5]. Because cross-regulation was described in the PRRs [30],
137 with nuclear accumulation of TOC1 depending partly on PRR5, it is likely that TOC1
138 contributes to the phenotype of PRR5-deficient mutant backgrounds. We also
139 characterized *PRR5* and *PRR7* expression in *prp79* and *prp59* double mutants,
140 respectively. Levels of *PRR5* and *PRR7* were ~1.5-fold higher in *prp59* and *prp79*
141 compared to WT, and *PRR5* phase was delayed in *prp79*, indicative of intricate cross-
142 regulatory pathways (Figure S2D). Significantly, *CDF5* expression in the *prp59* mutant
143 from ZT3-ZT21 was almost linear (Figure 3D), in accordance with the PRRs (with TOC1
144 possibly also contributing) being responsible for the repression of *CDF5* expression from
145 morning to midnight.

146 To further examine the PIF-PRR antagonistic interplay, we artificially induced PIF
147 accumulation at the beginning of the night period when PRR levels are high (Figure 3A)
148 [27] by giving a far-red light pulse (FRp) at ZT8 [5,28]. As control we used *PIL1*, a direct
149 PIF target and marker gene for PIF abundance and activity [8]. *PIL1* levels accumulated
150 in the WT immediately after the FRp (Figure 3E), in agreement with the rapid
151 accumulation of PIF proteins after a FRp [9,25,31], and to PRRs not interfering
152 significantly with PIF activity in the regulation of *PIL1*, in accordance with *PIL1* not
153 being a direct target of all PRRs [15]. In striking contrast, expression induction of the
154 PIF-PRR target *CDF5* was repressed in the WT during the first part of the night (ZT8-
155 ZT16) after a FRp, similarly to the control (-FRp) samples (Figure 3E). Interestingly, this
156 repression was much lower in *prp5* and *prp7*, and not observed in *prp59*. In *toc1*, early
157 *CDF5* expression compared to WT (Figures 3E and S2C) was more evident in (+FRp)
158 samples.

159 Although part of the effect seen in *prp* mutants might come from elevated PIF4/5 levels
160 due to their transcriptional derepression (Fig 2C), together these data support the
161 conclusion that the PRR9/7/5 and TOC1 prevent the transcriptional activation of *CDF5*
162 by PIFs. Given the sequential pattern of expression of *PRR9*, *7*, *5*, and *TOC1* (Figure 3A)
163 [21], and the progressive accumulation of the PIFs along the night in SD conditions [8],
164 our findings suggest that *CDF5* is sequentially targeted by *PRR9*, *7*, *5*, and *TOC1* to
165 repress its expression from morning to midnight (when PRR and TOC1 levels are high),
166 to gate PIF direct induction of *CDF5* to dawn when the levels of PRRs and TOC1 are low

167 and PIFs reach a peak in abundance. We propose that *CDF5* might be a novel target of
168 this PRR and PIF interplay in the promotion of hypocotyl elongation.

169 Our findings suggest a model where the antagonistic regulation of *CDF5* gene expression
170 by PRRs and PIFs described above might underlie rhythmic growth under SD. In
171 agreement, we observed correlation between the magnitude of hypocotyl length under our
172 SD conditions and *CDF5* levels in *prp* and *pifq* mutants (Figures S3A and S3B). To test
173 this model genetically, we generated seedlings ectopically expressing *CDF5* in a *cdf5*
174 mutant background (*CDF5OX*) (Figure S3C), and quantified the hypocotyl phenotype of
175 WT, *CDF5OX*, and *cdf5* lines under SD. *cdf5* mutants were slightly shorter than WT SD-
176 grown seedlings, whereas *CDF5OX* lines suppressed the *cdf5* phenotype and showed a
177 range from subtle to robustly elongated hypocotyls compared to WT (Figures 4A). We
178 analyzed the elongation rate of *cdf5* and *CDF5OX* lines under SD compared to WT
179 (Figure 4B). As described, the growth rate of WT seedlings is highest during the second
180 half of the night [2]. Elongation rate of *cdf5* seedlings was similar to WT during the day
181 and first part of the night, but it was reduced during the last part of the night, when *CDF5*
182 expression in the WT is maximum, consistent with their short phenotype. Interestingly,
183 elongation rate of *CDF5OX* seedlings was constantly high during the day and most part
184 of the night (Figure 4B). Together, our data suggest that transcriptional control of *CDF5*
185 expression by the PIFs and PRRs is a key regulatory mechanism in growth control.

186 Next, to genetically test the interplay between *CDF5*, PIFs and PRRs, we generated
187 *prp7cdf5*, *pifqcdf5* and *pifqCDF5OX* and mutants (Figure S3C) to study their hypocotyl
188 phenotypes. We observed that in SD the quintuple *pifqcdf5* mutant displayed a phenotype
189 similar to *pifq*, indicating that the *cdf5* mutation did not have an additive effect on *pifq*
190 mutation (Figure 4A). This result agrees with PIFq and *CDF5* acting in the same
191 signaling pathway. Overexpression of *CDF5* in the *pifq* background partially restored the
192 *pifq* phenotype (Figures 4A), providing additional evidence that *CDF5* contributes to
193 growth downstream of the PIFs. Finally, comparison of *prp7* with *prp7cdf5* mutants
194 showed that the long phenotype of *prp7* under SD is reduced when *CDF5* is removed in
195 *prp7cdf5* (Figures 4A), suggesting that exaggerated growth in *prp7* is partially a
196 consequence of having elevated levels of *CDF5*. Together, our results confirm our model

197 where PRRs and PIFs directly and antagonistically regulate *CDF5* expression to precisely
198 gate *CDF5* growth-promoting activity to the end of the night.
199 We hypothesized that *CDF5* might control the expression of growth-related genes at
200 dawn downstream of PIFq. We selected a few PIF-regulated [4], growth-related cell wall
201 [32] and SD growth-marker genes [6,8] to test for their expression in *cdf5* and *CDF5OX*
202 lines. As shown in Figure 4C, *PIL1* and *XTR7* were not significantly affected in *cdf5* or
203 *CDF5OX*, and *IAA19*, *YUCCA8* and three selected cell wall related genes (*AGP4*, *PME*,
204 and *FLA9*) show either significant down-regulation in *cdf5* (*IAA19*), up-regulation in
205 *CDF5OX* (*PME*, *AGP4*), or both (*YUC8* and *FLA9*), compared to the WT. Interestingly,
206 *AGP4* and *PME* are not PIF-bound genes. These results suggest branching downstream of
207 PIFq, with *CDF5* regulating a subset of the PIFq-regulated growth-related genes, in
208 accordance to the partial suppression of the *pifq* phenotype by *CDF5OX* shown above
209 (Figure 4A). Examination of the hypocotyl cell size in SD-grown WT, *cdf5* and *CDF5OX*
210 seedlings by confocal microscopy imaging clearly showed elongated cells in *CDF5OX*
211 hypocotyls compared to WT, whereas cells in *cdf5* appeared shorter (Figure 4D left),
212 which was confirmed by quantification of the hypocotyl cell length (Figure 4D right).
213 Next, we tested *prr7*, which exhibited a longer cell phenotype partially suppressed by
214 genetic removal of *CDF5* in *prr7cdf5* (Figure 4D). In contrast, cell length in *pifq* was
215 shorter than WT, a phenotype that was partially recovered by *CDF5OX* (Figure 4C right).
216 Together, these results support a role for *CDF5* in the promotion of cell elongation under
217 the inductive growth condition of SDs downstream of PRRs and PIFs.

218 **Conclusions**

219 Here we found that members of the PRR family of transcriptional repressors (PRR5, 7,
220 and 9), with a key role in the regulation of the central circadian oscillator and clock
221 output processes in plants [12], target growth-related genes that are directly induced by
222 the growth-promoting PIF transcription factors. Given the coincident DNA-binding
223 specificity of PRRs and PIFs (Figure 1A) [15,33], the PIF-PRR physical interaction in the
224 nucleus (Figures 1B and S1A), and their accumulation dynamics during short-day
225 photoperiods (Figure 3A) [2,7,8,11,21], we propose a model in which successive binding
226 of the PRR9, PRR7, and PRR5 to the G-box elements of shared PIF and PRR target
227 genes (like the growth-promoting *CDF5*) acts to sequentially repress transcription of the

228 PIF-induced transcriptional network starting in the morning (Figure 4E, Figure S4).
229 Given that PRR9/7/5 have not been shown to bind DNA directly, our results agree with
230 the possibility that PIFs might bridge the binding of PRRs to DNA, although competition
231 by direct binding of PRR to G-boxes, or through a PRR- and G-box- binding factor
232 different than PIFq, cannot be completely discarded based on our results. These findings
233 define an expanded framework for previous results showing PRR1/TOC1 repression of
234 PIF transcriptional activity at midnight [5]. At dawn, PRRs and TOC1 are not present,
235 PIF protein accumulation reaches a maximum, and elongation is promoted by PIF-
236 induced expression of growth-promoting genes like *CDF5* (Figure 4E). Collectively, our
237 data reveal that gating of growth occurs not only at the post-dusk hours of the night as
238 previously described for TOC1 [5], but instead starts in the morning and covers all the
239 day period until midnight through the sequential action of the PRR family of
240 transcriptional repressors. The molecular mechanism described here could explain why
241 growth rate under short-day photoperiods is low [2] from morning to midnight in the
242 presence of low PIF3 and PIF1 [9,34] and considerable high amounts of PIF4 (and likely
243 PIF5) [7,10], a regulation critical for fitness by preventing overgrowth (Figure 4A). Our
244 results reveal that gating of growth has evolved in plants to encompass the orchestrated
245 sequential action of members of the PRR family (PRR9/7/5/1) of transcriptional
246 repressors that peak in waves from morning to midnight. This function highlights the dual
247 role of the PRR family of clock oscillator components, as regulators of central clock
248 components and cycling outputs [11,21,35], and as repressors of the physiological output
249 of growth in combined regulation with light pathways that control accumulation of PIFs.

250 **Acknowledgements**

251 We thank D. Somers, S.Pratt, G. Coupland, and R. McClung for sharing seed and plasmid
252 resources. We thank G. Steele for generating double and triple *prp* mutants, and the *prp*
253 mutant combinations. The work in this manuscript was supported by grants from the
254 Spanish “Ministerio de Economía y Competitividad” (MINECO) BIO2012-31672 and
255 BIO2015-68460-P, and from the Generalitat de Catalunya 2014-SGR-1406 to E.M.; by
256 Marie Curie IRG PIRG06-GA-2009-256420 grant to P.L.; by the European Commission
257 (PCIG2012-GA-2012-334052) and by MINECO (BIO2015-70812-ERC; RYC-2011-

258 09220) to R.H.; by Royal Society Grant RG2016R1 to G. T-O; by MINECO BIO2013-
259 43184-P to D.A; by MINECO AGL2014-57200-JIN to E.G.M. We acknowledge
260 financial support by the CERCA programme/Generalitat de Catalunya and from
261 MINECO through the “Severo Ochoa Programme for Centers of Excellence in R&D”
262 2016-2019 (SEV-2015-0533)”.

263 **Author contributions**

264 G.M., P.L., and E.M. conceived and designed the study, G.M., A.R., N.V., J.S., G.T-O.,
265 C.M.M.G., M.B., R.H., E.G.M., D.A., K.H., P.L., and E.M. acquired, analyzed and
266 interpreted data. G.M., P.L., and E.M. wrote the manuscript.

267 **Declaration of Interests**

268 The authors declare no competing interests.

269 **References**

- 270 1. Niwa, Y., Yamashino, T., and Mizuno, T. (2009). The Circadian Clock Regulates
271 the Photoperiodic Response of Hypocotyl Elongation through a Coincidence
272 Mechanism in *Arabidopsis thaliana*. *Plant Cell Physiol.* *50*, 838–854.
- 273 2. Nozue, K., Covington, M.F., Duek, P.D., Lorrain, S., Fankhauser, C., Harmer,
274 S.L., and Maloof, J.N. (2007). Rhythmic growth explained by coincidence
275 between internal and external cues. *Nature* *448*, 358–361.
- 276 3. Nomoto, Y., Kubozono, S., Yamashino, T., Nakamichi, N., and Mizuno, T. (2012).
277 Circadian Clock- and PIF4-Controlled Plant Growth: A Coincidence Mechanism
278 Directly Integrates a Hormone Signaling Network into the Photoperiodic Control
279 of Plant Architectures in *Arabidopsis thaliana*. *Plant Cell Physiol.* *53*, 1950–1964.
- 280 4. Martín, G., Soy, J., and Monte, E. (2016). Genomic Analysis Reveals Contrasting
281 PIFq Contribution to Diurnal Rhythmic Gene Expression in PIF-Induced and -
282 Repressed Genes. *Front. Plant Sci.* *7*, 962.
- 283 5. Soy, J., Leivar, P., González-Schain, N., Martín, G., Diaz, C., Sentandreu, M., Al-
284 Sady, B., Quail, P.H., and Monte, E. (2016). Molecular convergence of clock and
285 photosensory pathways through PIF3–TOC1 interaction and co-occupancy of
286 target promoters. *Proc. Natl. Acad. Sci. U. S. A.* *113*, 4870–4875.
- 287 6. Nozue, K., Harmer, S.L., and Maloof, J.N. (2011). Genomic Analysis of Circadian
288 Clock-, Light-, and Growth-Correlated Genes Reveals PHYTOCHROME-
289 INTERACTING FACTOR5 as a Modulator of Auxin Signaling in *Arabidopsis*.

- 290 Plant Physiol. *156*, 357–372.
- 291 7. Bernardo-García, S., de Lucas, M., Martínez, C., Espinosa-Ruiz, A., Davière, J.-
292 M., and Prat, S. (2014). BR-dependent phosphorylation modulates PIF4
293 transcriptional activity and shapes diurnal hypocotyl growth. *Genes Dev.* *28*,
294 1681–1694.
- 295 8. Soy, J., Leivar, P., González-Schain, N., Sentandreu, M., Prat, S., Quail, P.H., and
296 Monte, E. (2012). Phytochrome-imposed oscillations in PIF3 protein abundance
297 regulate hypocotyl growth under diurnal light/dark conditions in *Arabidopsis*.
298 *Plant J.* *71*, 390–401.
- 299 9. Monte, E., Tepperman, J.M., Al-Sady, B., Kaczorowski, K.A., Alonso, J.M.,
300 Ecker, J.R., Li, X., Zhang, Y., and Quail, P.H. (2004). The phytochrome-
301 interacting transcription factor, PIF3, acts early, selectively, and positively in light-
302 induced chloroplast development. *Proc. Natl. Acad. Sci. U. S. A.* *101*, 16091–
303 16098.
- 304 10. Yamashino, T., Nomoto, Y., Lorrain, S., Miyachi, M., Ito, S., Nakamichi, N.,
305 Fankhauser, C., and Mizuno, T. (2013). Verification at the protein level of the
306 PIF4-mediated external coincidence model for the temperature-adaptive
307 photoperiodic control of plant growth in *Arabidopsis thaliana*. *Plant Signal. Behav.*
308 *8*, e23390.
- 309 11. Nakamichi, N., Kiba, T., Henriques, R., Mizuno, T., Chua, N.-H., and Sakakibara,
310 H. (2010). PSEUDO-RESPONSE REGULATORS 9, 7, and 5 Are Transcriptional
311 Repressors in the *Arabidopsis* Circadian Clock. *Plant Cell* *22*, 594–605.
- 312 12. Farré, E.M., and Liu, T. (2013). The PRR family of transcriptional regulators
313 reflects the complexity and evolution of plant circadian clocks. *Curr. Opin. Plant*
314 *Biol.* *16*, 621–629.
- 315 13. Nakamichi, N., Kita, M., Ito, S., Yamashino, T., and Mizuno, T. (2005).
316 PSEUDO-RESPONSE REGULATORS, PRR9, PRR7 and PRR5, Together Play
317 Essential Roles Close to the Circadian Clock of *Arabidopsis thaliana*. *Plant Cell*
318 *Physiol.* *46*, 686–698.
- 319 14. Kaczorowski, K.A., and Quail, P.H. (2003). *Arabidopsis* PSEUDO-RESPONSE
320 REGULATOR7 Is a Signaling Intermediate in Phytochrome-Regulated Seedling
321 Deetiolation and Phasing of the Circadian Clock. *Plant Cell* *15*, 2654–2665.
- 322 15. Liu, T.L., Newton, L., Liu, M.-J., Shiu, S.-H., and Farré, E.M. (2016). A G-Box-
323 Like Motif Is Necessary for Transcriptional Regulation by Circadian Pseudo-
324 Response Regulators in *Arabidopsis*. *Plant Physiol.* *170*, 528–539.
- 325 16. Pfeiffer, A., Shi, H., Tepperman, J.M., Zhang, Y., and Quail, P.H. (2014).
326 Combinatorial Complexity in a Transcriptionally Centered Signaling Hub in
327 *Arabidopsis*. *Mol. Plant* *7*, 1598–1618.

- 328 17. Martínez-García, J.F., Huq, E., and Quail, P.H. (2000). Direct Targeting of Light
329 Signals to a Promoter Element-Bound Transcription Factor. *Science* 288, 859–863.
- 330 18. Fornara, F., de Montaigu, A., Sánchez- Villarreal, A., Takahashi, Y., Ver Loren
331 van Themaat, E., Huettel, B., Davis, S.J., and Coupland, G. (2015). The GI–CDF
332 module of Arabidopsis affects freezing tolerance and growth as well as flowering.
333 *Plant J.* 81, 695–706.
- 334 19. Fornara, F., Panigrahi, K.C.S., Gissot, L., Sauerbrunn, N., Rühl, M., Jarillo, J.A.,
335 and Coupland, G. (2009). Arabidopsis DOF Transcription Factors Act
336 Redundantly to Reduce CONSTANS Expression and Are Essential for a
337 Photoperiodic Flowering Response. *Dev. Cell* 17, 75–86.
- 338 20. Zhu, J.-Y., Oh, E., Wang, T., and Wang, Z.-Y. (2016). TOC1–PIF4 interaction
339 mediates the circadian gating of thermoresponsive growth in Arabidopsis. *Nat.*
340 *Commun.* 7, 13692.
- 341 21. Matsushika, A., Makino, S., Kojima, M., and Mizuno, T. (2000). Circadian Waves
342 of Expression of the APRR1/TOC1 Family of Pseudo-Response Regulators in
343 Arabidopsis thaliana: Insight into the Plant Circadian Clock. *Plant Cell Physiol.*
344 41, 1002–1012.
- 345 22. Nakamichi, N., Kiba, T., Kamioka, M., Suzuki, T., Yamashino, T., Higashiyama,
346 T., Sakakibara, H., and Mizuno, T. (2012). Transcriptional repressor PRR5 directly
347 regulates clock-output pathways. *Proc. Natl. Acad. Sci. U. S. A.* 109, 17123–
348 17128.
- 349 23. Huang, W., Pérez-García, P., Pokhilko, A., Millar, A.J., Antoshechkin, I.,
350 Riechmann, J.L., and Mas, P. (2012). Mapping the Core of the Arabidopsis
351 Circadian Clock Defines the Network Structure of the Oscillator. *Science* 336, 75–
352 79.
- 353 24. Haudry, A., Platts, A.E., Vello, E., Hoen, D.R., Leclercq, M., Williamson, R.J.,
354 Forczek, E., Joly-Lopez, Z., Steffen, J.G., Hazzouri, K.M., *et al.* (2013). An atlas
355 of over 90,000 conserved noncoding sequences provides insight into crucifer
356 regulatory regions. *Nat Genet* 45, 891–898.
- 357 25. Lorrain, S., Allen, T., Duek, P.D., Whitelam, G.C., and Fankhauser, C. (2008).
358 Phytochrome-mediated inhibition of shade avoidance involves degradation of
359 growth-promoting bHLH transcription factors. *Plant J.* 53, 312–323.
- 360 26. Al-Sady, B., Ni, W., Kircher, S., Schäfer, E., and Quail, P.H. (2006).
361 Photoactivated Phytochrome Induces Rapid PIF3 Phosphorylation Prior to
362 Proteasome-Mediated Degradation. *Mol. Cell* 23, 439–446.
- 363 27. Fujiwara, S., Wang, L., Han, L., Suh, S.-S., Salomé, P.A., McClung, C.R., and
364 Somers, D.E. (2008). Post-translational Regulation of the Arabidopsis Circadian
365 Clock through Selective Proteolysis and Phosphorylation of Pseudo-response

- 366 Regulator Proteins. *J. Biol. Chem.* 283, 23073–23083.
- 367 28. Soy, J., Leivar, P., and Monte, E. (2014). PIF1 promotes phytochrome-regulated
368 growth under photoperiodic conditions in Arabidopsis together with PIF3, PIF4,
369 and PIF5. *J. Exp. Bot.* 65, 2925–2936.
- 370 29. Hayama, R., Sarid- Krebs, L., Richter, R., Fernández, V., Jang, S., and Coupland,
371 G. (2017). PSEUDO RESPONSE REGULATORS stabilize CONSTANS protein
372 to promote flowering in response to day length. *EMBO J.* 36, 904–918.
- 373 30. Wang, L., Fujiwara, S., and Somers, D.E. (2010). PRR5 regulates phosphorylation,
374 nuclear import and subnuclear localization of TOC1 in the Arabidopsis circadian
375 clock. *EMBO J.* 29, 1903–1915.
- 376 31. Shen, H., Moon, J., and Huq, E. (2005). PIF1 is regulated by light-mediated
377 degradation through the ubiquitin-26S proteasome pathway to optimize
378 photomorphogenesis of seedlings in Arabidopsis. *Plant J.* 44, 1023–1035.
- 379 32. Pelletier, S., Van Orden, J., Wolf, S., Vissenberg, K., Delacourt, J., Ndong, Y.A.,
380 Pelloux, J., Bischoff, V., Urbain, A., Mouille, G., *et al.* (2010). A role for pectin
381 de-methylesterification in a developmentally regulated growth acceleration in
382 dark-grown Arabidopsis hypocotyls. *New Phytol.* 188, 726–739.
- 383 33. Heyndrickx, K.S., de Velde, J. Van, Wang, C., Weigel, D., and Vandepoele, K.
384 (2014). A Functional and Evolutionary Perspective on Transcription Factor
385 Binding in Arabidopsis thaliana. *Plant Cell* 26, 3894-3910.
- 386 34. Huq, E., Al-Sady, B., Hudson, M., Kim, C., Apel, K., and Quail, P.H. (2004).
387 PHYTOCHROME-INTERACTING FACTOR 1 Is a Critical bHLH Regulator of
388 Chlorophyll Biosynthesis. *Science* 305, 1937–1941.
- 389 35. Kamioka, M., Takao, S., Suzuki, T., Taki, K., Higashiyama, T., Kinoshita, T., and
390 Nakamichi, N. (2016). Direct Repression of Evening Genes by CIRCADIAN
391 CLOCK-ASSOCIATED1 in the Arabidopsis Circadian Clock. *Plant Cell* 28, 696–
392 711.
- 393 36. Kikis, E.A., Khanna, R., and Quail, P.H. (2005). ELF4 is a phytochrome-regulated
394 component of a negative-feedback loop involving the central oscillator
395 components CCA1 and LHY. *Plant J.* 44, 300–313.
- 396 37. Leivar, P., Monte, E., Oka, Y., Liu, T., Carle, C., Castillon, A., Huq, E., and Quail,
397 P.H. (2008). Multiple Phytochrome-Interacting bHLH Transcription Factors
398 Repress Premature Seedling Photomorphogenesis in Darkness. *Curr. Biol.* 18,
399 1815–1823.
- 400 38. Khanna, R., Shen, Y., Marion, C.M., Tsuchisaka, A., Theologis, A., Schäfer, E.,
401 and Quail, P.H. (2008). The Basic Helix-Loop-Helix Transcription Factor PIF5
402 Acts on Ethylene Biosynthesis and Phytochrome Signaling by Distinct

- 403 Mechanisms. *Plant Cell* 19, 3915-3929.
- 404 39. Michael, T.P., Salomé, P.A., Yu, H.J., Spencer, T.R., Sharp, E.L., McPeck, M.A.,
405 Alonso, J.M., Ecker, J.R., and McClung, C.R. (2003). Enhanced Fitness Conferred
406 by Naturally Occurring Variation in the Circadian Clock. *Science* 302, 1049–1053.
- 407 40. Fujimori, T., Yamashino, T., Kato, T., and Mizuno, T. (2004). Circadian-
408 Controlled Basic/Helix-Loop-Helix Factor, PIL6, Implicated in Light-Signal
409 Transduction in *Arabidopsis thaliana*. *Plant Cell Physiol.* 45, 1078–1086.
- 410 41. Más, P., Alabadí, D., Yanovsky, M.J., Oyama, T., and Kay, S.A. (2003). Dual
411 Role of TOC1 in the Control of Circadian and Photomorphogenic Responses in
412 *Arabidopsis*. *Plant Cell* 15, 223–236.
- 413 42. Liu, T., Carlsson, J., Takeuchi, T., Newton, L., and Farré, E.M. (2013). Direct
414 regulation of abiotic responses by the *Arabidopsis* circadian clock component
415 PRR7. *Plant J.* 76, 101–114.
- 416 43. Nicol, J.W., Helt, G.A., Blanchard Steven G., J., Raja, A., and Loraine, A.E.
417 (2009). The Integrated Genome Browser: free software for distribution and
418 exploration of genome-scale datasets. *Bioinformatics* 25, 2730–2731.
- 419 44. Huang, D.W., Sherman, B.T., Tan, Q., Collins, J.R., Alvord, W.G., Roayaei, J.,
420 Stephens, R., Baseler, M.W., Lane, H.C., and Lempicki, R.A. (2007). The DAVID
421 Gene Functional Classification Tool: a novel biological module-centric algorithm
422 to functionally analyze large gene lists. *Genome Biol.* 8, R183.
- 423 45. Toledo-Ortiz, G., Johansson, H., Lee, K.P., Bou-Torrent, J., Stewart, K., Steel, G.,
424 Rodríguez-Concepción, M., and Halliday, K.J. (2014). The HY5-PIF Regulatory
425 Module Coordinates Light and Temperature Control of Photosynthetic Gene
426 Transcription. *PLoS Genet.* 10, e1004416.
- 427 46. Ni, M., Tepperman, J.M., and Quail, P.H. (1998). PIF3, a Phytochrome-Interacting
428 Factor Necessary for Normal Photoinduced Signal Transduction, Is a Novel Basic
429 Helix-Loop-Helix Protein. *Cell* 95, 657–667.
- 430 47. Wang, L., Kim, J., and Somers, D.E. (2013). Transcriptional corepressor
431 TOPLESS complexes with pseudoresponse regulator proteins and histone
432 deacetylases to regulate circadian transcription. *Proc. Natl. Acad. Sci. U. S. A.*
433 110, 761–766.
- 434 48. Tanaka, Y., Kimura, T., Hikino, K., Goto, S., Nishimura, M., Mano, S., and
435 Nakagawa, T. (2012). Gateway Vectors for Plant Genetic Engineering: Overview
436 of Plant Vectors, Application for Bimolecular Fluorescence Complementation
437 (BiFC) and Multigene Construction. InTech.
- 438 49. Martín, G., Leivar, P., Ludevid, D., Tepperman, J.M., Quail, P.H., and Monte, E.
439 (2016). Phytochrome and retrograde signalling pathways converge to

440 antagonistically regulate a light-induced transcriptional network. Nat. Commun. 7,
441 11431.

442

443

444 **Figure Legends**

445 **Figure 1. Analysis of coincident co-binding of PRRs and PIFs to dawn-phased genes**
446 **under SD identifies *CDF5* as a PIF- and PRR5/7/9-bound gene.** (A) (Left)
447 Comparison of PIF-bound [16] and PRR5-, 7- and/or PRR9-bound genes [15] (gene lists
448 provided in Dataset 1) defines three groups of genes: “PIF only” (1,384 genes), “PRR
449 only” (3,013 genes), and “PIF-PRR” (1,460 genes). (Middle) Percentage of PIF-bound
450 genes in genes bound by single or a combination of PRRs. (Right) Frequency of pairwise
451 distance in base pairs (bp) between the PIF- and PRR- binding sites in each of the “PIF-
452 PRR” co-bound genes. (B) BiFC assay of the PRRs and PIF3 fusions to N- and C-
453 terminal fragments of YFP, respectively, in transfected onion cells. The combinations of
454 PIF3-cYFP and TOC1-nYFP or pGW-nYFP were used as positive and negative control,
455 respectively. (Left) YFP fluorescence image. (Center) Bright-field image. (Right) Merge
456 of YFP fluorescence and bright-field image. (C) Expression phases in SD of gene sets
457 defined in (A): “PIF-PRR” (purple), “PRR only” (pink), and “PIF only” (yellow). Phases
458 are indicated on the circumference, and fold-change phase enrichment of genes
459 (count/expected) on the radius. Day is shown in yellow; night in gray. See also Figure
460 S1 and Dataset 1. (D) Comparison of PIF- [16], PRR5-, 7-, and PRR9-bound genes [15],
461 and “PIF/SD-induced” genes [4] (see Dataset 1 for details) (E) Visualization of ChIP-seq
462 and ChIP-qPCR data in the genomic region encompassing the *CDF5* locus co-bound by
463 PIFs, PRRs and TOC1. For PIF (orange), ChIP-seq tracks show the pile-up of all the
464 reads obtained from MACS analyses (model based for ChIP-seq) of the dataset from
465 each experiment [16]. Each corresponding WT-ChIP/input control is overlaid in dark
466 gray. For PRR (purple), filled rectangles indicate the PRR9, PRR7 and PRR5 peaks
467 defined by ChIP-seq in [15]. Empty rectangles indicate peaks only described by ChIP-
468 qPCR, in [22] for PRR9 and in Figure 2A for TOC1. Conserved non-coding sequences
469 (CNS) (blue) are defined in [24]. G- and PBE-box: vertical lines indicate motif positions.
470 See also Figure S1 and Dataset 1.

471 **Figure 2. PRR7 represses PIF3 ability to induce *CDF5* expression in SD.** (A) PRR7,
472 TOC1, PIF3, and PIF4 binding to the G-box containing region of the *CDF5* promoter at
473 ZT8, ZT14, and ZT24 under SD. For ChIP-qPCR analysis, samples of SD-grown
474 *pPRR7::PRR7-GFP* (PRR7-GFP), *pTOC1::TOC1:YFP* (TMG), *pPIF3::YFP:PIF3*

475 (YFP-PIF3), and *35S::PIF4-HA* (PIF4-HA), were harvested at the indicated times during
476 the third day and were immunoprecipitated using anti-GFP or anti-HA antibodies. Data
477 are from three independent ChIP experiments, and error bars indicate SE. Statistically
478 significant differences between mean values by Student's *t*-test relative to WT are shown
479 ($*P<0.05$; $**P<0.01$ and $***P<0.001$). n.s., not significant. WT controls were Col-0 for
480 YFP-PIF3, PIF4-HA, and PRR7-GFP, and C24 for TMG seedlings. Ab: samples
481 immunoprecipitated with antibody. No Ab: control samples immunoprecipitated without
482 antibody. (B) *CDF5* expression levels in WT, *pif3*, *pif4*, *pif5*, *prp7*, *prp7pif3*, *prp7pif4*,
483 *prp7pif5*, and PIF4-HA. Samples were harvested at ZT9 during the third day of growth
484 (ZT8 for PIF4-HA), analyzed by qRT-PCR and normalized to *PP2A*. Data are from three
485 independent biological replicates relative to WT set at one. Different letters denote
486 statistically significant differences among means by Tukey-b test ($P<0.05$). Error bars
487 indicate SE. (C) WT and *prp7* seedlings grown for 2 d in SD conditions were harvested
488 during the third day at the indicated times. Expression levels of *PIF3* and *PIF4* were
489 analyzed by qRT-PCR, and values were normalized to *PP2A*. Data plotted are mean \pm SE
490 relative to *PIF4* WT at ZT3 set at one, $n = 2$ independent biological experiments, each
491 assayed in triplicate. (D) PIF3 protein levels in 3-day old SD-grown WT and *prp7*
492 seedlings at ZT24. C-blue, coomassie blue; NS, non-specific bands. (E) Hypocotyl length
493 in seedlings as in (B) (except for PIF4-HA) grown for 3 days in SD. Different letters
494 denote statistically significant differences among means by Tukey-b test ($P<0.05$). Data
495 are means \pm SE of at least 50 seedlings. See also Figure S2.

496 **Figure 3. PRRs and PIFs antagonistically regulate *CDF5* to dawn-phase its**
497 **expression under diurnal SD conditions. (A)** Transcriptional waves of *PRR9/7/5* and
498 *TOC1* expression during the third day in SD at the indicated times. Each gene is
499 expressed relative to its maximum expression value set at one. (B-D) *CDF5* expression
500 in WT, *pif*, and *prp* analyzed by qRT-PCR (B) Expression in 2-day-old SD-grown
501 seedlings harvested during the third day at the indicated times in seedlings kept under SD
502 or moved to continuous light (LL). Data are relative to WT SD ZT3. (C) Expression in
503 3-day-old seedlings at ZT24 grown as in (B). Data are from two independent biological
504 replicates and are relative to WT samples set at one. Percentage is the contribution of
505 each PIF to *CDF5* expression in SD considering *pifq* and WT values as 0% and 100%,

506 respectively. Error bars indicate SE. **(D)** Expression in WT, *prp5*, *prp7*, *prp9*, *prp59*,
507 *prp79*, and *prp579* seedlings grown for 2 d in SD conditions during the third day at the
508 indicated times. Expression is relative to *CDF5* WT at ZT3. **(E)** *PIL1* and *CDF5*
509 expression in WT, *prp* and *toc1* analyzed by qRT-PCR. Two-day-old SD-grown
510 seedlings were treated with a 15-min far-red pulse (FRp) at ZT8 on the third day ((+) FRp
511 samples, in red), and harvested during the night at ZT9, ZT12, ZT16 and ZT20. (-) FRp
512 control samples (in black) did not receive a FRp. Data are relative to ZT8 set at one for
513 each genotype. (A-E) All samples were normalized to *PP2A*. (A-B, D-E) Data plotted
514 are mean \pm SE, n=2 independent biological experiments, each assayed in triplicate. See
515 also Figures S2 and S3.

516 **Figure 4. PRR- and PIF-mediated regulation of cell elongation requires CDF5.** **(A)**
517 Hypocotyl length of WT, *cdf5*, *CDF5OX*, *pifq*, *pifqCDF5OX*, *prp7*, and *prp7cdf5* grown
518 for 3 and 4 days in SD (left). Data are means \pm SE of at least 35 seedlings. Different
519 letters denote statistically significant differences among means by Tukey-b test ($P < 0.05$).
520 Visible phenotypes of 3-day-old seedlings are shown in the right. Scale bar = 5 mm. **(B)**
521 Hypocotyl elongation rate for WT, *cdf5* and *CDF5OX 5.7* under SD conditions. Seedling
522 growth was monitored every 2 hours during the third day. Average of 12 seedlings is
523 shown, and SE is indicated by the shaded area. **(C)** Expression of PIF-regulated growth
524 marker genes (top) and cell wall genes (bottom) in 3-day-old SD-grown WT, *cdf5* and
525 *CDF5OX 5.7* seedlings at ZT24, analyzed by qRT-PCR and normalized to *PP2A*. Data
526 are from three independent biological replicates normalized to WT set at one. Error bars
527 indicate SE. Statistically significant differences between mean values by Student's *t*-test
528 relative to WT are shown (* $P < 0.05$; ** $P < 0.01$ and *** $P < 0.001$). n.s., not significant. **(D)**
529 (Left) Visual phenotypes of cell area in 3d-old SD-grown WT, *cdf5* and *CDF5OX 5.7*
530 seedling hypocotyls. Scale bar = 200 μ m. (Right) Quantification of cell length in WT,
531 *cdf5*, *CDF5OX 5.7*, *pifq*, *pifqCDF5OX* (*pifqOX* in the figure), *prp7*, and *prp7cdf5*.
532 Seedlings were grown for 3 days in SD. Data are means \pm SE of at least 100 cells from
533 3-4 independent seedlings. Different letters or an asterisk denote statistically significant
534 differences among means by Tukey-b test ($P < 0.05$) or by *t*-test ($P < 0.05$), respectively.
535 **(E)** Model of the proposed role of PRRs as repressors of PIF activity to regulate cell
536 elongation through *CDF5*. PIFs bind to the *CDF5* promoter and induce *CDF5*

537 transcription in the absence of PRRs. If PRRs are present, PRRs repress PIF
538 transcriptional activity through direct PIF-PRR interaction. Based on current data, PRRs
539 and PIFs could bind to the same or different nearby G-boxes, or alternatively, PRRs
540 could bind indirectly to G-boxes through DNA-bound PIFs or other G-box and PRR-
541 binding factors. Sequential PRR9/7/5 and PRR1/TOC1 accumulation from morning to
542 midnight gate PIF-induction of *CDF5* to dawn, when it induces hypocotyl cell elongation
543 by upregulating growth-related genes like *YUC8*, or *FLA9*. See also Figures S3 and S4.

544 **STAR Methods**

545 **Contact for Reagent and Resource Sharing**

546 Further information and requests for resources and reagents should be directed to and will
547 be fulfilled by the Lead Contact, Elena Monte (elena.monte@cragenomica.es).

548 **Experimental Model**

549 The *Arabidopsis thaliana* (L.) accession Columbia (Col-0), C24, and mutants used here
550 were obtained from the mentioned references or generated in this work (See Key
551 Resources Table).

552 **Method Details**

553 Seedling Growth and Hypocotyl and Cell Measurements

554 *Arabidopsis thaliana* seeds used in this manuscript include the previously described *cdf5*-
555 *1* [19], *toc1-101* [36], *pPRR7::PRR7-GFP* (PRR7-GFP) [27], *pPIF3::YFP:PIF3* (YFP-
556 PIF3) [26], *p35S::PIF4-HA* [25], *pif1-1* [34], *pif3-3* [9], *pif4-2* [37], *pif5-3* [38], *pifq* [37],
557 *prp5-1*, *prp7-3*, and *prp9-1* [39], *pif3-1* [9], *pif4-101* [25], *pil6-1* (*pif5* mutant) [40], and
558 the newly generated *prp7-3pif3-1* (*prp7pif3*), *prp7-3pif4-101* (*prp7pif4*), *prp7-3pil6-1*
559 (*prp7pif5*), *prp7-3prp9-1* (*prp79*), *prp5-1prp9-1* (*prp59*), *prp5-1prp7-3prp9-1* (*prp579*), and
560 *prp7-3cdf5-1* (*prp7cdf5*) in Col-0 ecotype, and *pTOC1::TOC1:YFP* (TMG) [41] in C24
561 ecotype. *CDF5OX* lines were generated by cloning the *CDF5* ORF under the regulation
562 of the 35S promoter in the pH7FWG2 vector. The resulting 35S::*CDF5*-GFP construct
563 was transformed into *cdf5* to generate *CDF5OX* lines, and into *pifq* to generate
564 *pifqCDF5OX* lines.

565 Seeds were sterilized and plated on Murashige and Skoog medium without sucrose.
566 Seedlings were stratified for 4d at 4C in darkness, and seedling growth was done in short
567 days (8h light + 16h dark) or continuous white light ($85\mu\text{mol}\cdot\text{m}^{-2}\cdot\text{s}^{-1}$) for the time
568 indicated in each experiment. Hypocotyl measurements in Figures 2E, 4A and S3B were
569 done using Image J (National Institutes of Health). Saturating FR pulses were $30\mu\text{mol}\cdot\text{m}^{-2}\cdot\text{s}^{-1}$
570 for 15min. Samples at ZT0 and ZT24 were collected in the dark, whereas at ZT8
571 were in the light. For hypocotyl growth rate measurements (Figure 4B), image acquisition
572 was done using the ActiveWebCam software (www.pysoft.com) under infrared light
573 background using modified webcams (Microsoft Life Cam Studio). Twelve seedlings
574 were measured individually every 2 hours throughout the diurnal cycle, the difference in
575 hypocotyl length between the two time points was calculated, and the elongation rate was
576 expressed as mm/h. The mean and SE for the 12 seedlings are represented. Cell size was
577 visualized in seedlings stained with propidium iodine ($10\mu\text{g}/\text{ml}$) (Calbiochem) using a
578 confocal laser microscope Leica SP5 (570 nm-666 nm). Cell length was measured in
579 pictures taken with an optic microscope (AixoPhot DP70) (Figure 4D).

580 ChIP-seq Data Analysis and Visualization

581 Comparison of ChIP-seq data shown in Figure 1A was performed using PIF- [16] and
582 PRR9/7/5-associated peaks from [15], which contained novel PRR9 and re-analyzed
583 ChIP-seq data for PRR5 [22] and PRR7 [42], considering only the PRR binding sites
584 located upstream of the transcriptional start site TSS as in [16]. The same comparison
585 was performed in Figure 1D adding the PIF/SD-induced gene set from [4]. Distance
586 between PIF and PRR peaks was calculated separately for all the different pair-wise
587 combinations associated to a given gene. To jointly visualize the Chip-Seq data for PRR
588 [15] and PIFs [16], and the conserved noncoding sequences (CNS) regions [24] (Figure
589 1E), the Integrated Genome Browser (IGB) [43] was used. Data was obtained from
590 <http://mustang.biol.mcgill.ca> (CNS), GSE71397 (PRRs) and GSE43286 (PIFs).
591 Expression phases shown in Figures 1C and S1C were analyzed using the PHASER tool
592 (<http://phaser.mocklerlab.org>) for SD (Col-0_SD), LD (longday), and LL (LL23_LDHH).
593 The PHASER tool generated over-representation p-values for each phase (Dataset 1).
594 DAVID system [44] was used to identify enriched GO biological terms (Figure S1B).

595 Chromatin Immunoprecipitation (ChIP) Assays

596 Chromatin immunoprecipitation (ChIP) and ChIP-qPCR assays (Figure 2A) were
597 performed as in [5,45]. For PIF3-YFP, all process was performed in the dark under green
598 safelight. Seedlings (3g) were vacuum-infiltrated with 1% formaldehyde and cross-
599 linking was quenched by vacuum infiltration with 0.125 M glycine for 5 min. Tissue was
600 ground, and nuclei-containing cross-linked protein and DNA were purified by sequential
601 extraction on Extraction Buffer 1 (0.4M Sucrose, 10 mM Tris-HCL pH8, 10mM MgCl₂,
602 5mM β-mercaptoethanol, 0.1mM PMSF, 50 μM MG132, proteinase inhibitor cocktail),
603 Buffer 2 (0.25M Sucrose, 10mM Tris-HCL pH8, 10mM MgCl₂, 1% Triton X-100, 5mM
604 β-mercaptoethanol, 0.1mM PMSF, 50 μM MG132, proteinase inhibitor cocktail), and
605 Buffer 3 (1.7M Sucrose, 10 mM Tris-HCL pH8, 0.15% Triton X-100, 2mM MgCl₂, 5mM
606 β-mercaptoethanol, 0.1mM PMSF, 50 μM MG132, proteinase inhibitor cocktail). Nuclei
607 were resuspended in nuclei lysis buffer (50 mM Tris-HCL pH8, 10 mM EDTA, 1 %
608 SDS, 50 μM MG132, proteinase inhibitor cocktail), sonicated for 10X 30sec, and diluted
609 10X in Dilution Buffer (0.01% SDS, 1% Triton X-100, 1.2 mM EDTA, 16.7 mM Tris-
610 HCL pH8, 167 mM NaCl). Overnight incubation was performed with the corresponding
611 antibody (or with no antibody as control) at 4C overnight, and immunoprecipitation was
612 performed using dynabeads. Washes were done sequentially in Low Salt Buffer (0.1%
613 SDS, 1% Triton X-100, 2 mM EDTA, 20 mM Tris-HCL pH8, 150 mM NaCl), High Salt
614 Buffer (0.1% SDS, 1% Triton X-100, 2 mM EDTA, 20 mM Tris-HCL pH8, 500 mM
615 NaCl), LiCl Buffer (0.25M LiCl, 1% NP40, 1% deoxycholic acid sodium, 1 mM EDTA,
616 10 mM Tris-HCL pH8), and TE X1. Immunocomplexes were eluted in Elution Buffer
617 (1%SDS, 0.1M NaHCO₃), de-crosslinked overnight at 65C in 10 mM NaCl, and then
618 treated with proteinase K. DNA was purified using Qiagen columns, eluted in 100 uL of
619 Qiagen elution buffer, and 2 uL were used for qPCR (ChIP-qPCR) using *CDF5*
620 promoter-specific primers (Table S1) spanning the region containing the predicted
621 binding sites for the PIFs [16]. Three biological replicates were performed for all the
622 “Antibody” samples (two for WT TMG at ZT8), and one for the “No Antibody”.
623 Calculations of percent input were done following the protocol available at
624 www.thermofisher.com.

625 Yeast Two-Hybrid Assays

626 For yeast two-hybrid assays shown in Figure S1A, we used PIF3 (pGAD424) and PIF4
627 (pGADT7) described previously [7,46]. PRR fragments were PCR-amplified from PRR
628 templates [47] with primers containing restriction sites (XmaI/BamHI for PRR5 and
629 PRR9, EcoRI/XmaI for PRR7) (Table S1), cloned into pTOPO vector (NZYTech),
630 sequenced and cloned into pGBKT7 (Clontech). To assess interactions, constructs were
631 co-transformed into yeast AH109 cells (Clontech). Yeast transformants were selected on
632 synthetic dropout medium (SD) deficient in leucine and tryptophan (-LT), and interaction
633 was assayed quantitatively by a β -Galactosidase assay performed using ortho-
634 nitrophenyl- β -D-galacpyranoside as a substrate following manufacturer's instructions.

635 Bimolecular Fluorescence Complementation (BiFC) Assays

636 For bimolecular fluorescence complementation (BiFC) shown in Figure 1B, the coding
637 regions of PIF3 and TOC1 [5] were cloned into pGWcY and pGWnY vectors [48],
638 respectively. PRR5-, PRR7- and PRR9-nYFP are from [47]. Preparation of samples and
639 bombardment of onion cells were done as in [5]. Briefly, the inner layers of spring onions
640 were cut in 2 x 2 cm squares and used for particle bombardment. Each sample was
641 transfected with 1 μ g of each plasmid coupled to tungsten particles using a Biolistic
642 Particle Delivery System PDS-1000 (Bio-Rad). After bombardment, onions were
643 exposed to a saturating 15 min FR pulse and incubated overnight in dark conditions. The
644 upper epidermal layer was removed, placed in a microscope slide and visualized using a
645 confocal laser scanning microscope Olympus FV1000 (Objective Lens UPLSAPO 20X,
646 Laser Wavelength: 514 nm, Emission window: 525-600 nm).

647 Protein Extraction and Immunoblot

648 Total protein extracts to detect endogenous PIF3 were prepared from 3 day-old SD-
649 grown seedlings harvested at ZT24 in the dark (Figure 2D). Total protein extracts to
650 detect endogenous PIF3 were prepared from 3 day-old SD-grown seedlings harvested at
651 ZT24 in the dark (Figure 2D). Extraction buffer and protein quantification were done
652 essentially as described [49]: Samples were collected and frozen in liquid nitrogen, and
653 manually ground under frozen conditions before resuspension in boiling extraction buffer
654 (100 mM MOPS (pH 7.6), 2% SDS, 10% glycerol, 4mM EDTA, 50mM Sodium
655 metabisulfite ($\text{Na}_2\text{S}_2\text{O}_5$), 2 g l^{-1} aprotinin, 3 g l^{-1} leupeptin, 1 g l^{-1} pepstatin and 2 mM

656 PMSF). Total protein was quantified using a Protein DC kit (Bio-Rad), and β -
657 mercaptoethanol was added just before loading. Aliquots of 100 ug for each sample were
658 treated for 5min at 95C and subjected to 12.5% SDS- PAGE gels. Proteins were then
659 transferred to Immobilon-P membrane (Millipore), and immunodetection of endogenous
660 PIF3 was performed using a anti-PIF3 antibody [26] (1:10,000 dilution) incubated with
661 Hikari solution (Nacalai Tesque). Peroxidase-linked anti rabbit secondary antibody
662 (1:5,000 dilution) and a SuperSignal West Femto chemiluminescence kit (Pierce) were
663 used for detection of luminescence using LAS-4000 Image imaging system (Fujifilm).
664 The membrane was stained with Coomassie blue as a loading control.

665 Gene Expression Analysis

666 Quantitative RT-PCR, RNA extraction, cDNA synthesis and qRT-PCR were done as
667 described [49]. Briefly, 1 mg of total RNA extracted using the RNeasy Plant Mini Kit
668 (Qiagen) were treated with DNase I (Ambion) according to the manufacturer's
669 instructions. First-strand cDNA synthesis was performed using the SuperScript III
670 reverse transcriptase (Invitrogen) and oligo dT as a primer (dT30). cDNA was then
671 treated with RNase Out (Invitrogen) before 1:20 dilution with water, and 2 ul was used
672 for real-time PCR (Light Cycler 480; Roche) using SYBR Premix Ex Taq (Takara) and
673 primers at a 300 nM concentration. Gene expression in time-course analyses (Figures 2C,
674 3A, 3B, 3D, 3E, S2C and S2D) was measured in two independent biological replicates,
675 with three technical replicates for each biological sample, and the mean of the biological
676 replicates \pm SE is shown. For specific time points in Figures 2B, 4C, S2A, S2B, and S3C,
677 gene expression was measured in three independent biological replicates, and in Figure
678 3C, corresponds to two biological replicates, with three technical replicates for each
679 biological sample. *PP2A* (*ATIG13320*) was used for normalization.

680 **Quantification and Statistical Analysis**

681 Differences between means were statistically analyzed by one-way analysis of variance
682 using Tukey-b post hoc multiple comparison test (IBM SPSS Statistics Software) or
683 homoscedastic Student's t-test (Excel Microsoft), as indicated in the figure legends.
684 Statistically significant differences were defined as those with a P value < 0.05.
685 Significance level is indicated as * P < 0.05, ** P < 0.01 and *** P < 0.001.

686 **Supplemental Tables**

687 Dataset 1: Comparison of genome-wide loci associated to PIFs and PRR9, 7 and 5.
688 Related to Figure 1.

689 Table S1: List of Oligonucleotides. Related to STAR Methods.

690

TABLE FOR AUTHOR TO COMPLETE

Please upload the completed table as a separate document. **Please do not add subheadings to the Key Resources Table.** If you wish to make an entry that does not fall into one of the subheadings below, please contact your handling editor. (NOTE: For authors publishing in *Current Biology*, please note that references within the KRT should be in numbered style, rather than Harvard.)

KEY RESOURCES TABLE

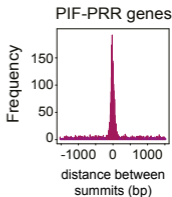
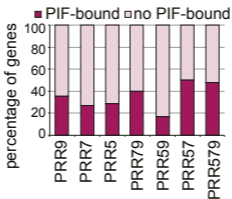
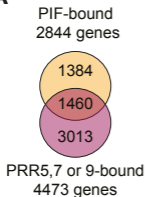
REAGENT or RESOURCE	SOURCE	IDENTIFIER
Antibodies		
Anti-GFP	Invitrogen	Cat# A11122
Peroxidase-linked anti rabbit secondary antibody	Sigma	Cat# NA934
Anti-PIF3	[26]	N/A
Anti-HA	Abcam	Cat# 9110
Bacterial and Virus Strains		
AH109	Clontech	N/A
<i>E. coli</i> DH5 α	N/A	N/A
<i>A. tumefaciens</i> GV3031	N/A	N/A
Chemicals, Peptides, and Recombinant Proteins		
Formaldehyde	ThermoFisher Scientific	Cat# 28908
Glycine	GE Healthcare Life Sciences	Cat# 17-1323-01
EDTA	Thermo Scientific	Cat# 17892
Tris-HCL	Sigma	Cat# C4706-2G
Proteinase K	ThermoFisher Scientific	Cat# EO0491
Sucrose	Applichem	Cat# A1125.1000
MgCl ₂	Calbiochem	Cat# 442611
PMSF	Applichem	Cat# A0999,0025
MG132	Merck	Cat# 474790
Proteinase Inhibitor Cocktail	Roche	Cat# 4693116001
Triton X-100	Applichem	Cat# A1388.10000
NaCl	Scharlau	Cat# SO02271000
LiCl	Merck	Cat# 1,056,790,250
NP40	Sigma	Cat# 74385
Deoxycholic acid sodium	Sigma	Cat# D6750
NaHCO ₃	Merck	Cat# 6329
Dropout medium (-AHLT)	Clontech	Cat# 630428
Yeast Nitrogen Base w/o aa & ammonium sulfate	Conda	Cat# 1553.00
Ammonium Sulfate	Sigma	Cat# A4418
D-Glucose	Applichem	Cat# 3O000431
European bacteriological Agar	Conda	Cat# 1800.00
His	Sigma	Cat# H8125
Trp	Sigma	Cat# T0254
Leu	Sigma	Cat# L8912
Ade	Sigma	Cat# A9126

Propidium iodine	Calbiochem	Cat# 537059-
Ortho-nitrophenyl- β -D-galacpyranoside	ThermoFisher Scientific	Cat# 34055
DNase I	Ambion	Cat# AM2224
RNase Out	Invitrogen	Cat# 10777019
SYBR Premix Ex Taq	Roche	Cat# 04707516001
MOPS (pH 7.6)	Sigma	Cat# M1254
SDS	Amresco	Cat# 0227
Glycerol	Applichem	Cat# A2926
EDTA	Thermo Scientific	Cat# 17892
Aprotinin	Applichem	Cat# A2132
Leupeptin	Applichem	Cat# A2183
Pepsatin	Applichem	Cat# A2205
PMSF	Applichem	Cat# A0999
β -mercaptoethanol	Fluka	Cat# 03700
GFP Agarose Beads	MBL	Cat# D153-8
rProtein A-Sepharose	Bionova	Cat# 1-888-752-2568
Hikari solution	Nacalai Tesque	Cat# 02270-81
Sodium metabisulfite	Sigma	Cat# 255556
XmaI	Roche	Cat# ER0171
BamHI	Roche	Cat# 10 220 612 001
EcoRI	Roche	Cat# 10 703 737 001
T4 DNA Ligase	NZYtech	Cat# MB00703
BP Clonase II	Gateway	Cat# 11789-020
LR Clonase II	Gateway	Cat# 11791-020
Critical Commercial Assays		
RNeasy Plant Mini	Qiagen	Cat# 74904
SuperScript III reverse transcriptase	Invitrogen	Cat# 18080044
Protein DC	Bio-Rad	Cat# 5000121
SuperSignal West Femto chemiluminescence	Thermo Scientific	Cat# 34095
QIAquick gel extraction kit	Qiagen	Cat# QIA28704
Dynabeads	Invitrogen	Cat# 10004D
Immobilon-P membrane	Millipore	Cat# IPVH00010
Experimental Models: Organisms/Strains		
Col-0	N/A	N/A
C24	N/A	N/A
<i>cdf5-1</i>	[19]	N/A
<i>toc1-101</i>	[36]	N/A
<i>pPRR7::PRR7-GFP</i> (PRR7-GFP)	[27]	N/A
<i>pPIF3::YFP:PIF3</i> (YFP-PIF3)	[26]	N/A
<i>p35S::PIF4-HA</i> (PIF4-HA)	[25]	N/A
<i>pTOC1::TOC1:YFP</i> (TMG)	[41]	N/A
<i>pif1-1</i>	[34]	N/A
<i>pif3-3</i>	[9]	N/A
<i>pif4-2</i>	[37]	N/A

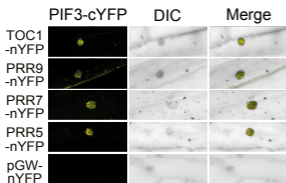
<i>pif5-3</i>	[38]	N/A
<i>pifq</i>	[37]	N/A
<i>prp5-1</i>	[39]	N/A
<i>prp7-3</i>	[39]	N/A
<i>prp9-1</i>	[39]	N/A
<i>pif3-1</i>	[9]	N/A
<i>pif4-101</i>	[25]	N/A
<i>pil6-1 (pif5)</i>	[40]	N/A
<i>prp7-3pif3-1 (prp7pif3)</i>	This paper	N/A
<i>prp7-3pif4-101 (prp7pif4)</i>	This paper	N/A
<i>prp7-3pil6-1 (prp7pif5)</i>	This paper	N/A
<i>prp7-3prp9-1 (prp79)</i>	This paper	N/A
<i>prp5-1prp9-1 (prp59)</i>	This paper	N/A
<i>prp5-1prp7-3prp9-1 (prp579)</i>	This paper	N/A
<i>prp7-3cdf5-1 (prp7cdf5)</i>	This paper	N/A
<i>35S::CDF5-GFP (CDF5OX)</i>	This paper	N/A
<i>pifqCDF5OX</i>	This paper	N/A
<i>pifqcdf5</i>	This paper	N/A
Oligonucleotides		
See Table S2	N/A	N/A
Recombinant DNA		
pH7FWG2	Gateway	N/A
PIF3 in pGAD424	[46]	N/A
PIF4 in pGADT7	[7]	N/A
NZY-A PCR cloning kit	NZYTech	Cat# MB05302
pGBKT7	Clontech	Cat# PT3248-5
pGWcY	[48]	N/A
pGWnY	[48]	N/A
Software and Algorithms		
ActiveWebCam software (www.pysoft.com)	N/A	N/A
Integrated Genome Browser (IGB)	[43]	N/A
PHASER (http://phaser.mocklerlab.org)	N/A	N/A
DAVID system	[44]	N/A
IBM SPSS Statistics Software	N/A	N/A
Excel	N/A	N/A

Figure 1

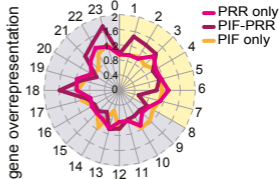
A



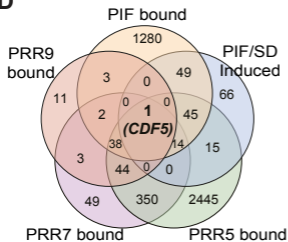
B



C



D



E

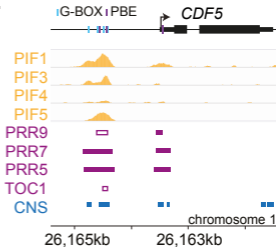
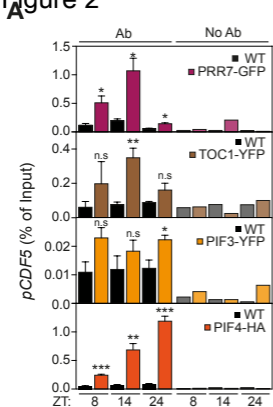
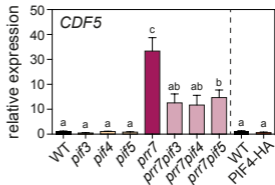


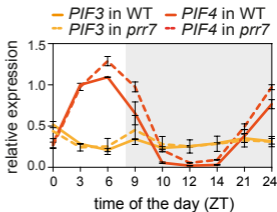
Figure 2



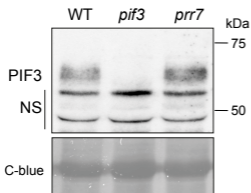
B



C



D



E

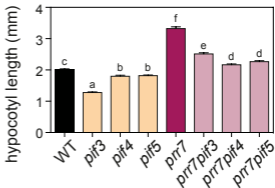


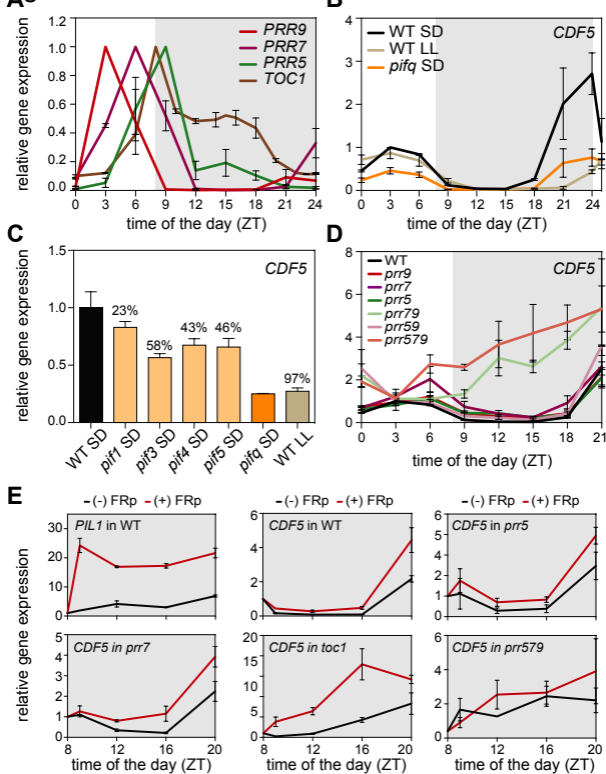
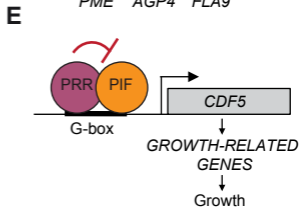
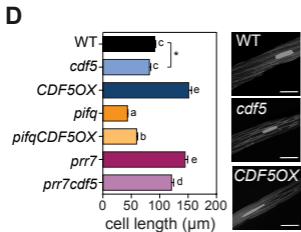
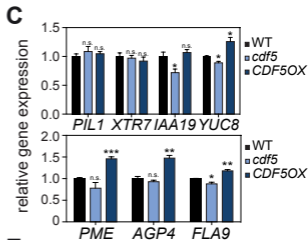
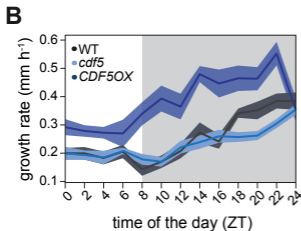
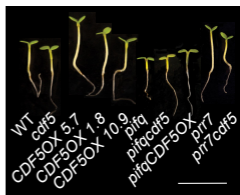
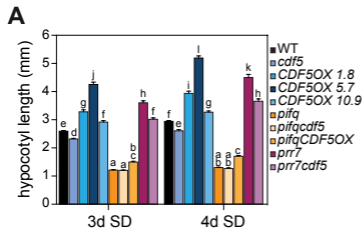
Figure 3

Figure 4



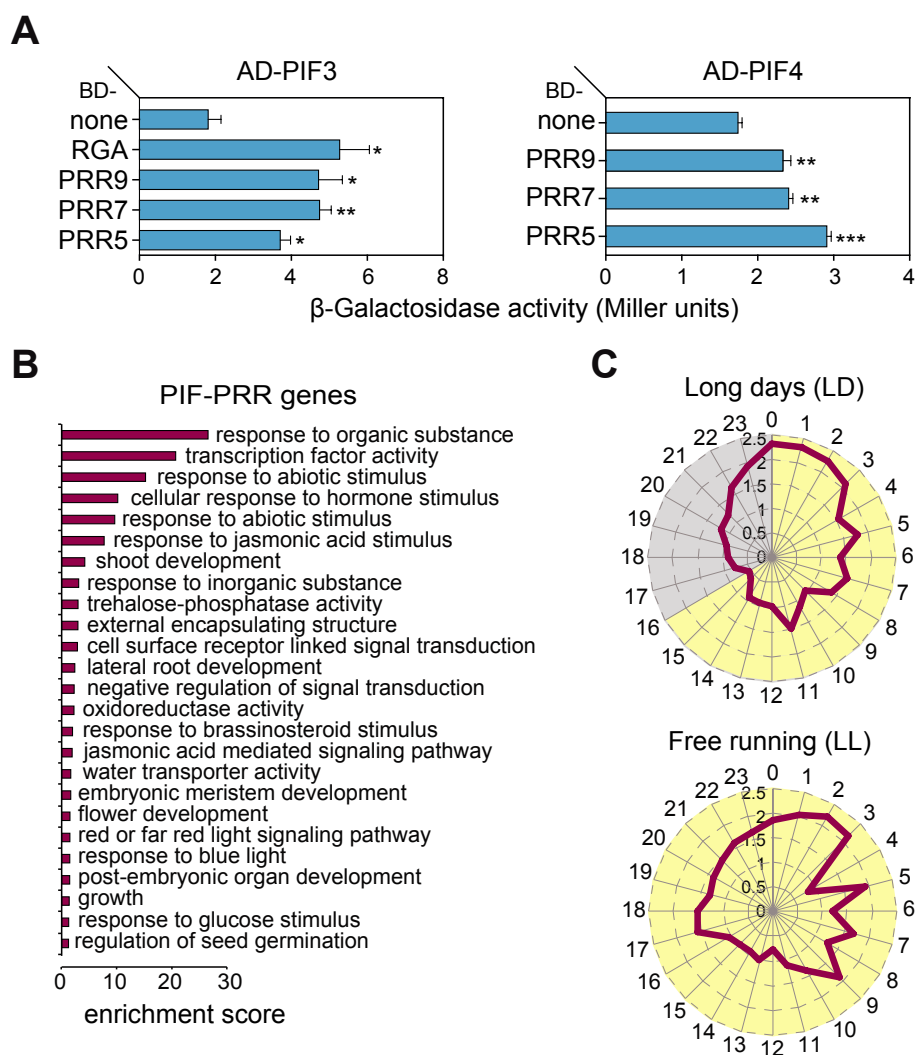


Figure S1. Related to Figure 1. Yeast-two-hybrid assays showing the interaction between PIF3, PIF4, and PRR9/7/5, and gene ontology (GO) and phaser analysis in LD and LL of PIF-PRR genes. (A) β -galactosidase activities from yeast two-hybrid assays showing interactions between PIF3 (left), PIF4 (right) and PRR5, PRR7, and PRR9. Error bars indicate SE ($n = 3$). Significance level is relative to the BD alone control (* $P < 0.05$; ** $P < 0.01$ and *** $P < 0.001$). DELLA protein RGA is included as positive control for PIF3 interactions [S1]. **(B)** Cluster analysis of the most enriched GO annotations for PIF-PRR genes. **(C)** Comparison of expression phases in long days (top) and free running (bottom) conditions of the 1,460 “PIF-PRR” gene set defined in Figure 1A and provided in Dataset 1. Phases as defined by PHASER (phaser.mocklerlab.org) are indicated on the circumference, and fold-change phase enrichment of genes (count/expected) is shown on the radius. Day is shown in yellow; night is shown in grey.

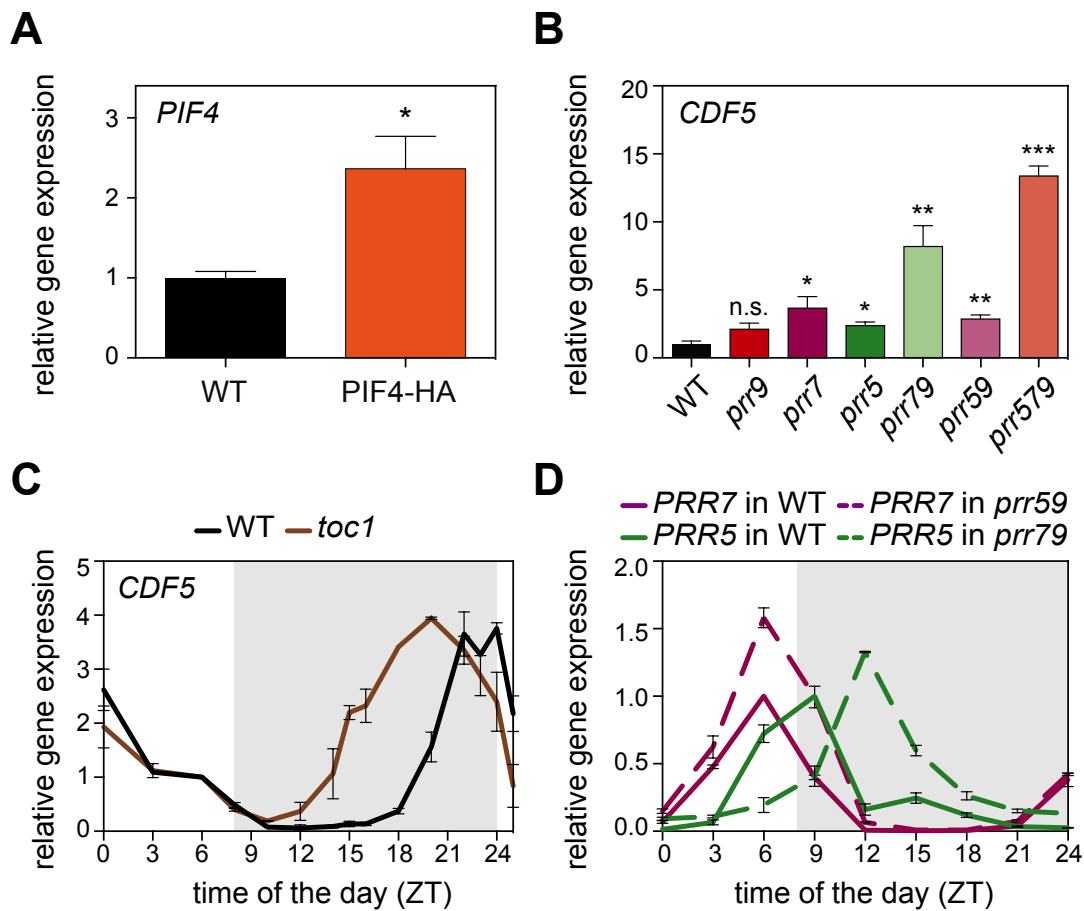


Figure S2. Related to Figures 2 and 3. *PIF4*, *CDF5*, *PRR5* and *PRR7* expression analyses in *PIF4*-HA overexpressing plants, and in *toc1*, *prr5*, *prr7*, and *prr9* single and higher order mutant combinations. *PIF4* expression in WT and *35S::PIF4-HA* (*PIF4*-HA) seedlings at ZT8 (A) and *CDF5* expression in WT and *prr* mutants at ZT9 (B) during the third day of growth in SD. Data are from three independent biological replicates relative to WT set at one. Error bars indicate SE. Statistically significant differences between mean values by Student's *t*-test relative to WT are shown (* $P < 0.05$; ** $P < 0.01$ and *** $P < 0.001$). n.s., not significant. (C) *CDF5* expression in WT and *toc1*. (D) *PRR5* and *PRR7* expression in WT and *prr79* and *prr59*, respectively. (C, D) Seedlings were grown for 2 days in SD and harvested during the third day at the indicated times. Data plotted are mean \pm SE relative to ZT6 for each genotype (C) or relative to its maximum expression value set at one for each gene (D), $n = 2$ independent biological experiments, each assayed in triplicate. (A-D) All samples were analyzed by qRT-PCR and normalized to *PP2A*.

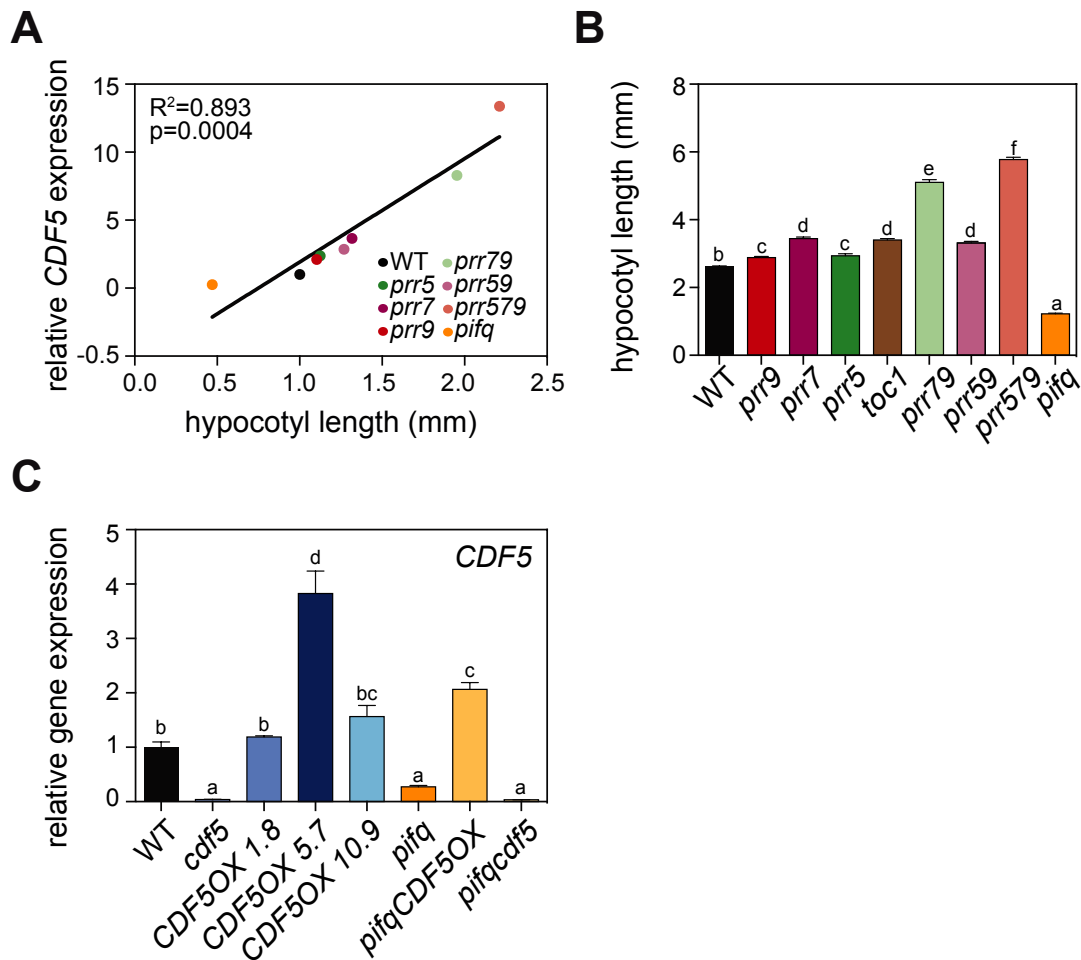


Figure S3. Related to Figures 3 and 4. *CDF5* expression in correlation with hypocotyl length and in generated *CDF5* mutant lines. (A) *CDF5* expression levels correlate with hypocotyl length. Correlation of hypocotyl length in (B) with *CDF5* expression values of WT, *prp* and *toc1* in 2-day-old SD-grown seedlings harvested at ZT9 during the third day under SD. *pifq* expression values are from Figure S2A. (B) Quantification of hypocotyl elongation in 3-day-old SD-grown WT, *prp*, *toc1*, and *pifq* seedlings. Data are means \pm SE of at least 50 seedlings. (C) Characterization of *CDF5* expression levels in *CDF5OX* mutant lines. *CDF5* expression in 3-d-old SD-grown WT, *cdf5*, *CDF5OX*, *pifq*, *pifqCDF5OX*, and *pifqcdf5* seedlings at ZT24. In (A) and (C), expression was analyzed by qRT-PCR, and values were normalized to *PP2A* and are shown relative to WT levels set at one. Data are from three independent biological replicates. In (C) error bars indicate SE. Different letters shown in (B) and (C) denote statistically significant differences among means by Tukey-b test ($P < 0.05$).

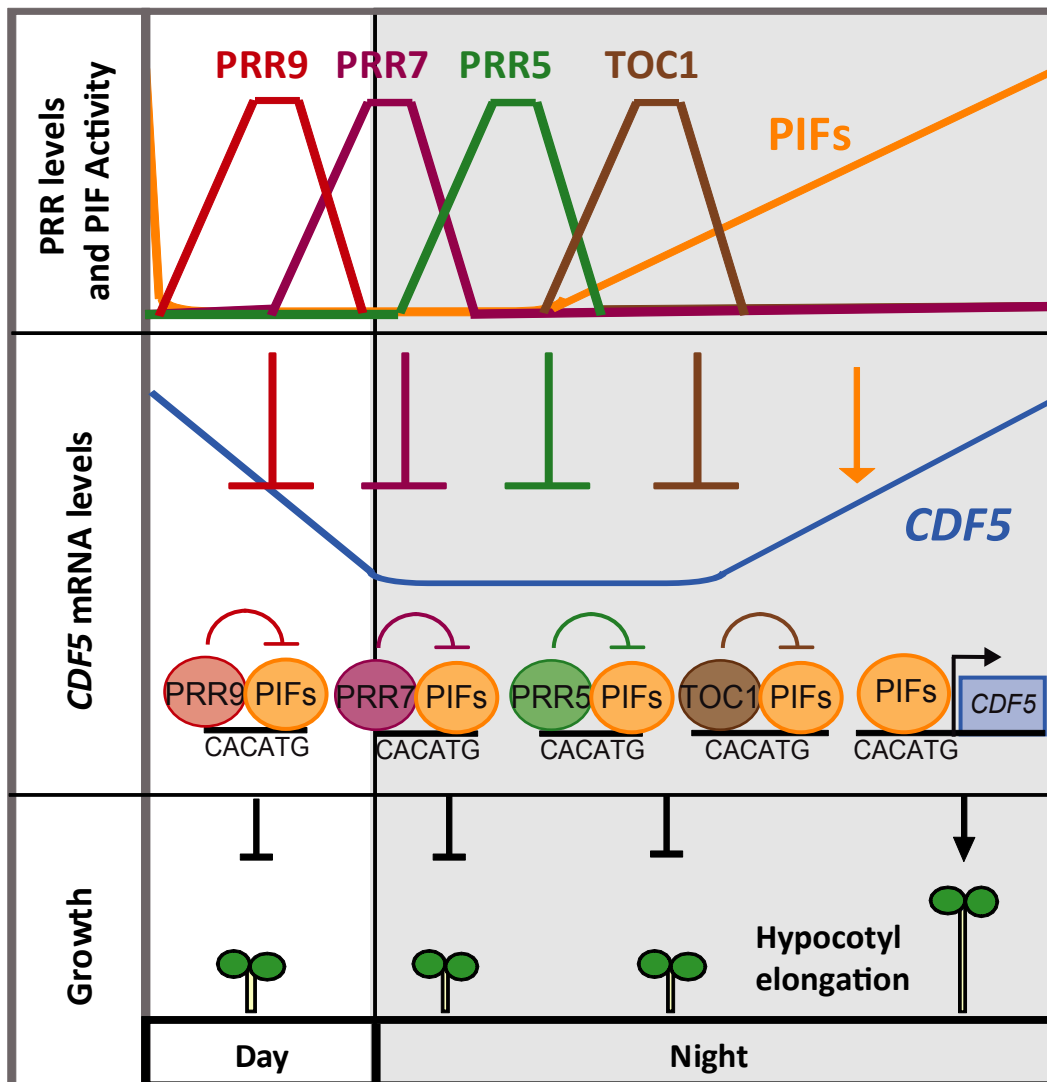


Figure S4. Related to Figure 4. Model of the proposed role of PRRs as repressors of PIF activity in gating CDF5-mediated elongation. Sequential PRR9/7/5 and PRR1/TOC1 accumulation from morning to midnight (top) represses PIF-induction of *CDF5*, a transcription factor necessary for growth-promotion (middle). PIFs are present during the day and progressively accumulate during the night concurrently to a decline in PRRs and TOC1 abundance (top). At predawn, PRRs and TOC1 are no longer present, repression on the PIFs is lifted (top), and PIFs induce *CDF5* expression (middle) to promote hypocotyl elongation (bottom). Based on current data, PRRs and PIFs could bind to the same or different nearby G-boxes, PIFs might bridge the binding of PRRs to DNA, or PRRs could compete with PIFs for binding to G-boxes.

Supplemental References

- S1. Feng, S., Martinez, C., Gusmaroli, G., Wang, Y., Zhou, J., Wang, F., Chen, L., Yu, L., Iglesias-Pedraz, J.M., Kircher, S., *et al.* (2008). Coordinated regulation of *Arabidopsis thaliana* development by light and gibberellins. *Nature* *451*, 475–479.
- S2. Pfeiffer, A., Shi, H., Tepperman, J.M., Zhang, Y., and Quail, P.H. (2014). Combinatorial Complexity in a Transcriptionally Centered Signaling Hub in *Arabidopsis*. *Mol. Plant* *7*, 1598–1618.
- S3. Liu, T.L., Newton, L., Liu, M.-J., Shiu, S.-H., and Farré, E.M. (2016). A G-Box-Like Motif Is Necessary for Transcriptional Regulation by Circadian Pseudo-Response Regulators in *Arabidopsis*. *Plant Physiol.* *170*, 528–539.
- S4. Martín, G., Soy, J., and Monte, E. (2016). Genomic Analysis Reveals Contrasting PIFq Contribution to Diurnal Rhythmic Gene Expression in PIF-Induced and - Repressed Genes. *Front. Plant Sci.* *7*, 962.
- S5. Fornara, F., Panigrahi, K.C.S., Gissot, L., Sauerbrunn, N., Rühl, M., Jarillo, J.A., and Coupland, G. (2009). *Arabidopsis* DOF Transcription Factors Act Redundantly to Reduce *CONSTANS* Expression and Are Essential for a Photoperiodic Flowering Response. *Dev. Cell* *17*, 75–86.
- S6. Mockler, T.C., Yu, X., Shalitin, D., Parikh, D., Michael, T.P., Liou, J., Huang, J., Smith, Z., Alonso, J.M., Ecker, J.R., *et al.* (2004). Regulation of flowering time in *Arabidopsis* by K homology domain proteins. *Proc. Natl. Acad. Sci. U. S. A.* *101*, 12759–12764.
- S7. Soy, J., Leivar, P., González-Schain, N., Martín, G., Diaz, C., Sentandreu, M., Al-Sady, B., Quail, P.H., and Monte, E. (2016). Molecular convergence of clock and photosensory pathways through PIF3–TOC1 interaction and co-occupancy of target promoters. *Proc. Natl. Acad. Sci. U. S. A.* *113*, 4870–4875.
- S8. Soy, J., Leivar, P., González-Schain, N., Sentandreu, M., Prat, S., Quail, P.H., and Monte, E. (2012). Phytochrome-imposed oscillations in PIF3 protein abundance regulate hypocotyl growth under diurnal light/dark conditions in *Arabidopsis*. *Plant J.* *71*, 390–401.
- S9. http://www.tdx.cat/bitstream/handle/10803/130896/MGR_TESIS.pdf.
- S10. Rawat, R., Schwartz, J., Jones, M.A., Sairanen, I., Cheng, Y., Andersson, C.R., Zhao, Y., Ljung, K., and Harmer, S.L. (2009). *REVEILLE1*, a Myb-like transcription factor, integrates the circadian clock and auxin pathways. *Proc. Natl. Acad. Sci. U. S. A.* *106*, 16883–16888.
- S11. Shin, J., Park, E., and Choi, G. (2007). PIF3 regulates anthocyanin biosynthesis in an HY5-dependent manner with both factors directly binding anthocyanin biosynthetic gene promoters in *Arabidopsis*. *Plant J.* *49*, 981–994.